

Review

Open Access



Recent advances in elevated-temperature flexible composite dielectrics for energy storage applications

Liang Zhao¹, Fan Zhang^{1,2}, Hailong Hu³

¹School of Minerals Processing and Bioengineering, Central South University, Changsha 410083, Hunan, China.

²Hunan Key Laboratory of Mineral Materials and Application, Central South University, Changsha 410083, Hunan, China.

³Research Institute of Aerospace Technology, Central South University, Changsha 410083, Hunan, China.

Correspondence to: Dr. Fan Zhang, School of Minerals Processing and Bioengineering, Central South University, Changsha 410083, Hunan, China; Hunan Key Laboratory of Mineral Materials and Application, Central South University, Changsha 410083, Hunan, China. E-mail: fan.zhang@csu.edu.cn; Dr. Hailong Hu, Research Institute of Aerospace Technology, Central South University, Changsha 410083, China. No. 932, Yuelu District, Lushan South Road, Changsha 410083, Hunan, China. Email: hailonghu@csu.edu.cn

How to cite this article: Zhao, L.; Zhang, F.; Hu, H. Recent advances in elevated-temperature flexible composite dielectrics for energy storage applications. *Microstructures* 2025, 5, 2025085. <https://dx.doi.org/10.20517/microstructures.2025.14>

Received: 12 Feb 2025 **First Decision:** 26 Mar 2025 **Revised:** 29 Apr 2025 **Accepted:** 30 Apr 2025 **Published:** 22 Jul 2025

Academic Editor: Shujun Zhang **Copy Editor:** Shu-Yuan Duan **Production Editor:** Shu-Yuan Duan

Abstract

Dielectric composites play a crucial role in meeting the growing demand for high-energy-density capacitors that can operate effectively in challenging environments. These applications include aerospace power management, underground oil and gas exploration, electrified transportation, and pulse power systems. This work provides a comprehensive overview of current research on flexible, high-temperature-resistant composite dielectrics for energy storage, emphasizing enhancing thermal stability and dielectric performance. Initially, this work examines the crucial characterization parameters that define the performance of dielectric energy storage materials at elevated temperatures and explores the mechanisms behind them. Subsequently, the recent research achievements and the primary challenges facing these flexible composite materials are summarized. Further discussions on strategies are performed for optimizing the microstructure of these materials to improve performance, where three key dimensions are analyzed, such as system selection, filler types, and structural design. Additionally, the review introduces innovative approaches to enhance the temperature resistance of flexible dielectric composites, employing machine learning algorithms and high entropy design concepts. Finally, a summary and future outlook on the potential development pathways in this field are concluded.

Keywords: Composite dielectrics, energy storage, flexible electronics, elevated temperature applications



© The Author(s) 2025. **Open Access** This article is licensed under a Creative Commons Attribution 4.0 International License (<https://creativecommons.org/licenses/by/4.0/>), which permits unrestricted use, sharing, adaptation, distribution and reproduction in any medium or format, for any purpose, even commercially, as long as you give appropriate credit to the original author(s) and the source, provide a link to the Creative Commons license, and indicate if changes were made.



INTRODUCTION

With the rapid development of modern electronics and power systems, dielectric energy storage capacitors have gained significant attention due to their unique capability of ultra-fast charge/discharge cycles (millisecond timescale)^[1-2]. However, their relatively low energy density compared to electrochemical storage devices presents a major challenge for applications requiring compact and miniaturized designs^[3]. This limitation becomes particularly critical in emerging industries operating under extreme conditions, where dielectric capacitors must maintain stable performance at elevated temperatures ranging from 150 °C to 300 °C or higher. Representative applications include hybrid/electric vehicle power systems (operating at ≈ 140 -150 °C), aerospace electronics (≈ 150 -350 °C), and downhole tools for oil/gas exploration (≈ 170 -250 °C)^[4-5]. Furthermore, the growing demand for flexible electronics necessitates dielectric materials that can withstand repeated bending and deformation without compromising functionality, especially for applications in confined or irregular spaces^[6]. These combined requirements highlight the urgent need for developing advanced flexible dielectric materials that simultaneously offer high energy storage density and exceptional thermal stability.

Capacitor dielectrics include both inorganic and polymeric materials, with polymer films representing $\sim 50\%$ of the global high-voltage market due to their superior flexibility, processability, and electrical properties [Figure 1]^[7]. Although ceramic dielectrics demonstrate exceptional high-temperature stability (withstanding several hundred °C), their brittleness and moderate breakdown strength [electrochemical breakdown (E_b)] pose significant limitations, with no flexible variants currently available for electrostatic energy storage. In contrast, polymer dielectrics excel in high-voltage applications through their high E_b , low dissipation factor ($\tan \delta$), and excellent charge/discharge efficiency (η), while offering additional advantages in lightweight design and voltage scalability^[8-9]. Biaxially oriented polypropylene (BOPP) exemplifies these benefits with its cost-effectiveness and robust performance, though its utility is constrained by thermal limitations (> 85 °C) and low dielectric constant ($\epsilon_r \approx 2.2$), which restrict energy density (U_d) in high-temperature applications^[10-11]. To overcome these challenges, composite dielectrics have emerged as a promising solution, combining multiple materials to enhance ϵ_r , minimize energy loss, and improve thermal/voltage stability, thereby enabling reliable performance across diverse operating conditions^[12-13].

This work presents advancements in the research of flexible composite dielectric energy storage materials and devices that exhibit high-temperature resistance. As shown in Figure 2, the study first introduces the key parameters used to characterize the performance of high-temperature dielectric energy storage mechanisms. It then discusses the latest developments and current bottlenecks in the field of flexible, high-temperature-resistant composite dielectric energy storage materials and devices. The structural design of these materials is explored from three aspects: system selection, filler selection, and structural configuration. Additionally, a new strategy is proposed to enhance high-temperature resistance in flexible composite dielectric energy storage materials. Finally, the paper provides a summary and an outlook on the future opportunities and challenges in this area of research.

CRUCIAL PARAMETERS AND ENERGY STORAGE MECHANISMS FOR HIGH-TEMPERATURE COMPOSITE DIELECTRICS

Dielectric properties

In the case of a linear dielectric, where polarization is directly proportional to the electric field, the energy density (U_e) stored within the material exhibits a linear dependence on the dielectric constant. Additionally, it demonstrates a quadratic relationship with the applied electric field, which can be mathematically expressed as follows^[14]

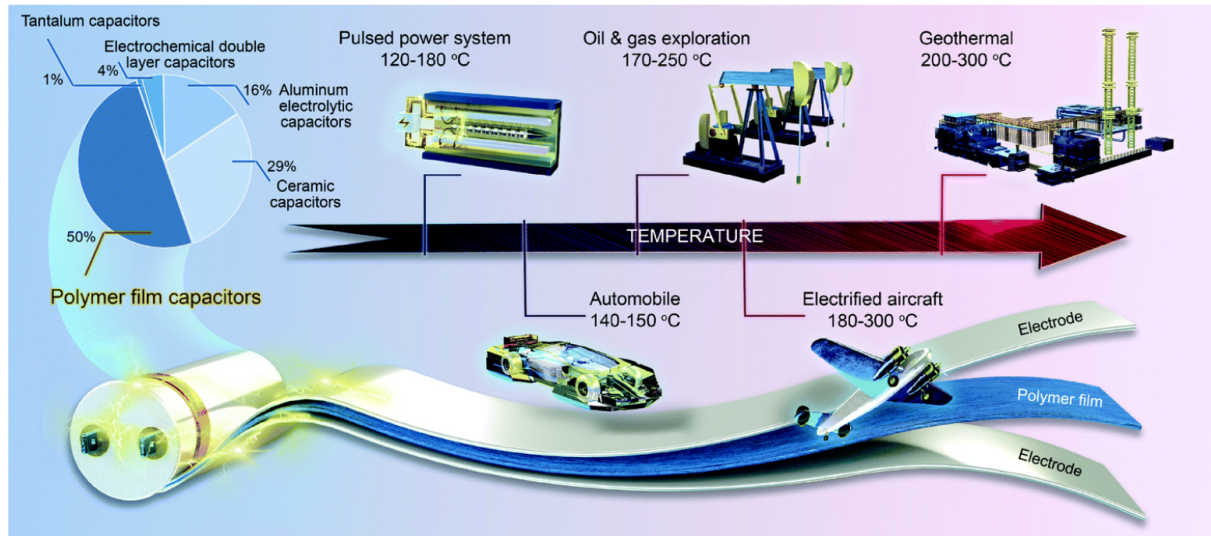


Figure 1. Global market share of high-voltage capacitors and applications of high-temperature dielectric polymer film capacitors^[7].

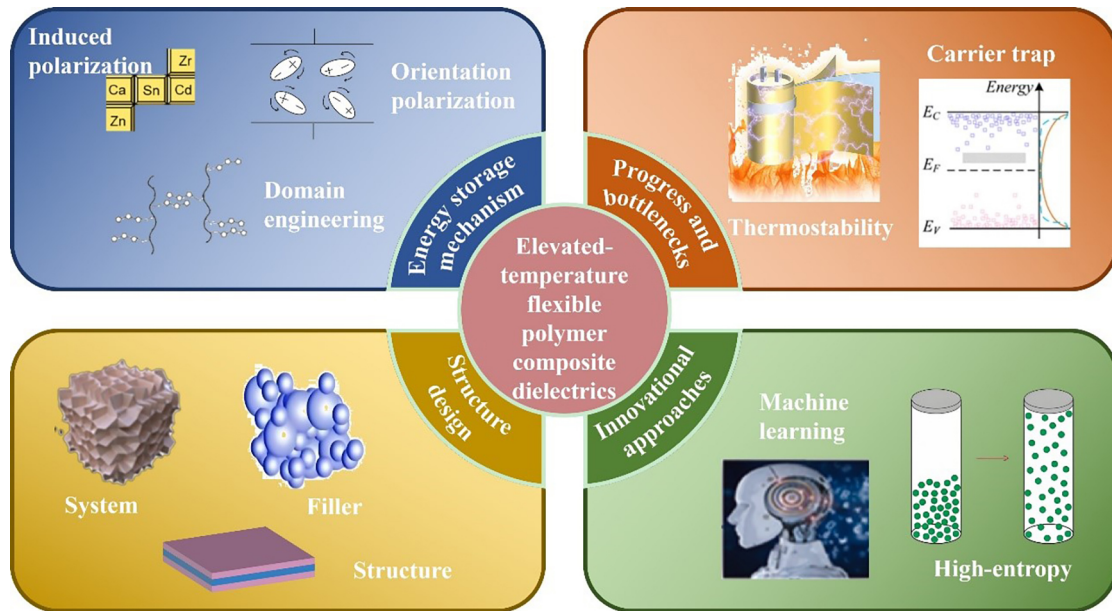


Figure 2. General framework and main content of this work.

$$U_e = \frac{1}{2} \epsilon_0 \epsilon E_b^2 \quad (1)$$

where ϵ_0 is the vacuum dielectric constant, ϵ is the dielectric constant of the dielectric material. The U_e stored within a capacitor is directly proportional to the dielectric constant of the material. Therefore, enhancing the dielectric constant can lead to an increase in U_e . This improvement enables the design of smaller and lighter capacitors, addressing the increasing demand for highly integrated, compact, and miniaturized electronic and power systems.

Dielectric loss, commonly referred to as the dissipation factor or the tangent of the loss angle ($\tan \delta$), serves as a parameter indicating the energy loss that occurs during the polarization and depolarization processes of a dielectric material^[15]. Dielectric loss adversely impacts both the U_d and η of capacitors, while simultaneously producing waste heat. Consequently, it is essential to enhance the dielectric constant while minimizing dielectric loss. The polarization characteristics of dielectric materials are influenced by temperature and frequency, leading to temperature and frequency-dependent variations in both dielectric constant and loss. Thus, for dielectric materials intended for operation across a broad spectrum of temperatures and frequencies, a minimal dependence of dielectric properties on these factors is imperative.

High-temperature dielectric energy storage mechanisms

Polarization mechanisms

Polarization significantly contributes to the energy storage capabilities of dielectric materials^[16-17]. It is defined as the vector sum of dipole moments generated by electric dipoles within a unit volume of the dielectric. The polarization P is related to the relative dielectric constant ϵ_r . The related equation is given below:

$$P = (\epsilon_r - 1)\epsilon_0 E \quad (2)$$

The total polarization of a dielectric is the sum of different polarization mechanisms including electronic polarization, ionic polarization, dipolarization, and interfacial polarization^[18], as shown in Figure 3.

The mechanism of electronic polarization is shown in Figure 4A. Electronic polarization occurs when an external electric field displaces electrons relative to atomic nuclei, thereby generating a dipole moment. Once the electric field is removed, this common yet weak effect disappears^[20-21].

Ionic polarization [Figure 4B] arises when an electric field displaces cations and anions asymmetrically, enhancing net polarization. This mechanism significantly boosts the high ϵ_r in ceramics like BaTiO_3 ^[21-24].

Dipole polarization [Figure 4C] involves the alignment of internal dipoles under an electric field. Polymers benefit from polar groups, which improve dielectric properties^[25-27].

Interface polarization [Figure 4D] results from charge accumulation at interfaces (e.g., polymer-filler, electrode-dielectric), which is crucial for high ϵ_r in composites. Multilayer structures optimize this effect^[25-27].

Charge injection and storage mechanism

Under certain conditions, an external electric field can inject charges into a composite dielectric, where traps (e.g., defects, impurities) capture and store them for energy storage. When the electric field is removed, charges may be slowly released. Optimizing trap density and distribution - via nanofillers or surface modification - enhances charge control and improves energy storage performance.

Mechanisms Related to Ferroelectricity and Antiferroelectricity

If the composite dielectric contains components of ferroelectric or antiferroelectric materials, its energy storage mechanism will involve the movement of electric domains and polarization reversal. In ferroelectrics, external fields rotate domains, enhancing polarization; residual polarization may remain after field removal. Antiferroelectric materials switch to a ferroelectric phase under fields, enabling abrupt polarization changes for energy storage. Combining these materials with dielectrics can optimize U_e and η .

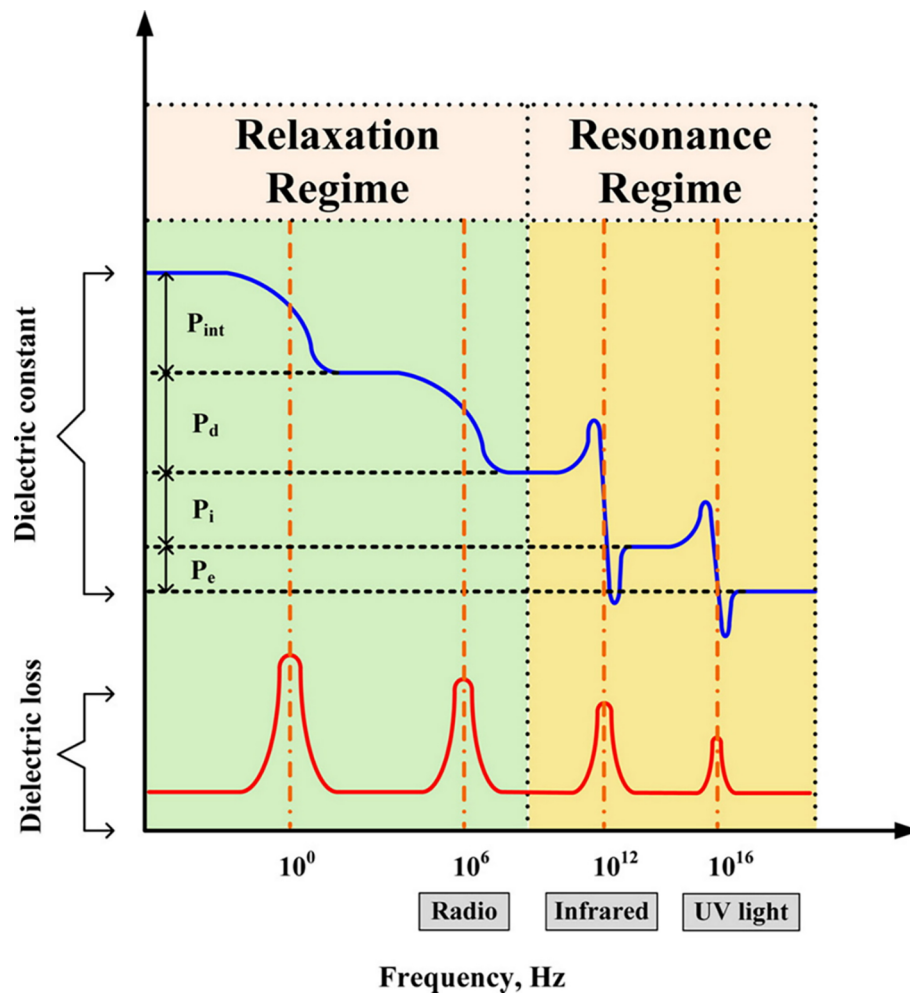


Figure 3. Four types of polarization and their frequency dependence. p_e , p_i , p_d , and p_{int} denote the electronic, ionic, dipole, and interfacial polarization, respectively^[19].

Strategies for engineering dielectric constant construction

Based on physical mechanisms, methods to construct intrinsic polymer dielectrics with controllable electrical properties fall into three main aspects: induced polarization modulation, polarization orientation modulation, and domain engineering (e.g., Figure 5). This involves polarized atoms, metal complexes, dipole mobility, arrangement, free volume, and ferroelectric/conducting domain orientation. Mastering these enables designing polymers with desired ϵ_r values, opening up more opportunities in energy storage, flexible electronics, smart sensing, human-computer interaction, and 5G/6G communications.

Modulation of induced polarization

The intensity of induced polarization (induced polarization) includes both electronic and ionic/atomic polarization. The Clausius-Mossotti equation $\frac{\epsilon_r - 1}{\epsilon_r + 2} = \frac{1}{3\epsilon_0} \sum_j N_j \alpha_j$ shows that induced polarization in a non-polar isotropic dielectric produces ϵ_r independent of the applied electric field, where N_j represents the number of atoms or molecules within a unit volume, while α_j denotes the material's polarizability^[29]. However, the polarizability of an atom is influenced by factors such as electron density and atomic radius. Specifically, an increase in the number of electrons, along with a greater distance between the electrons and

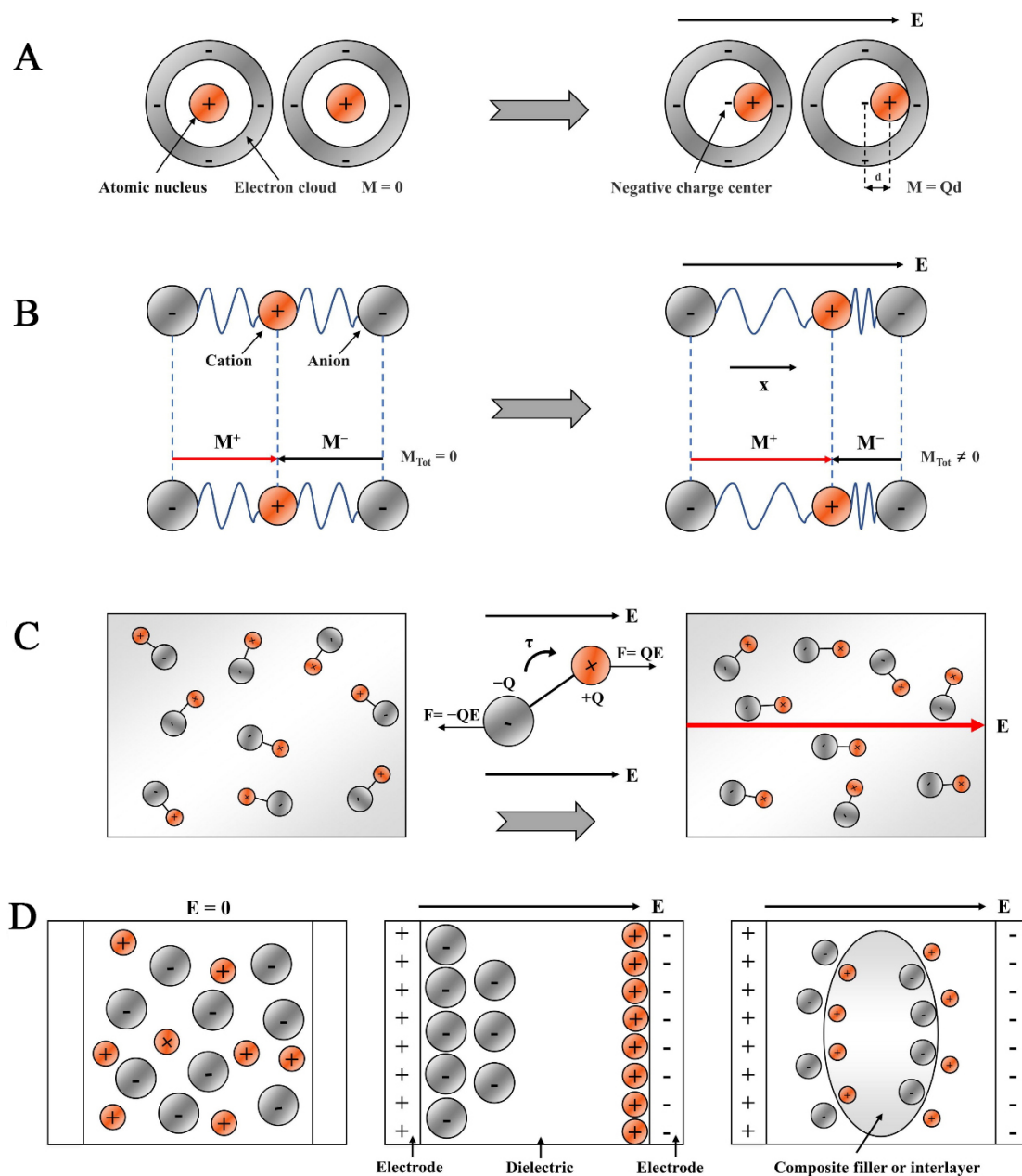
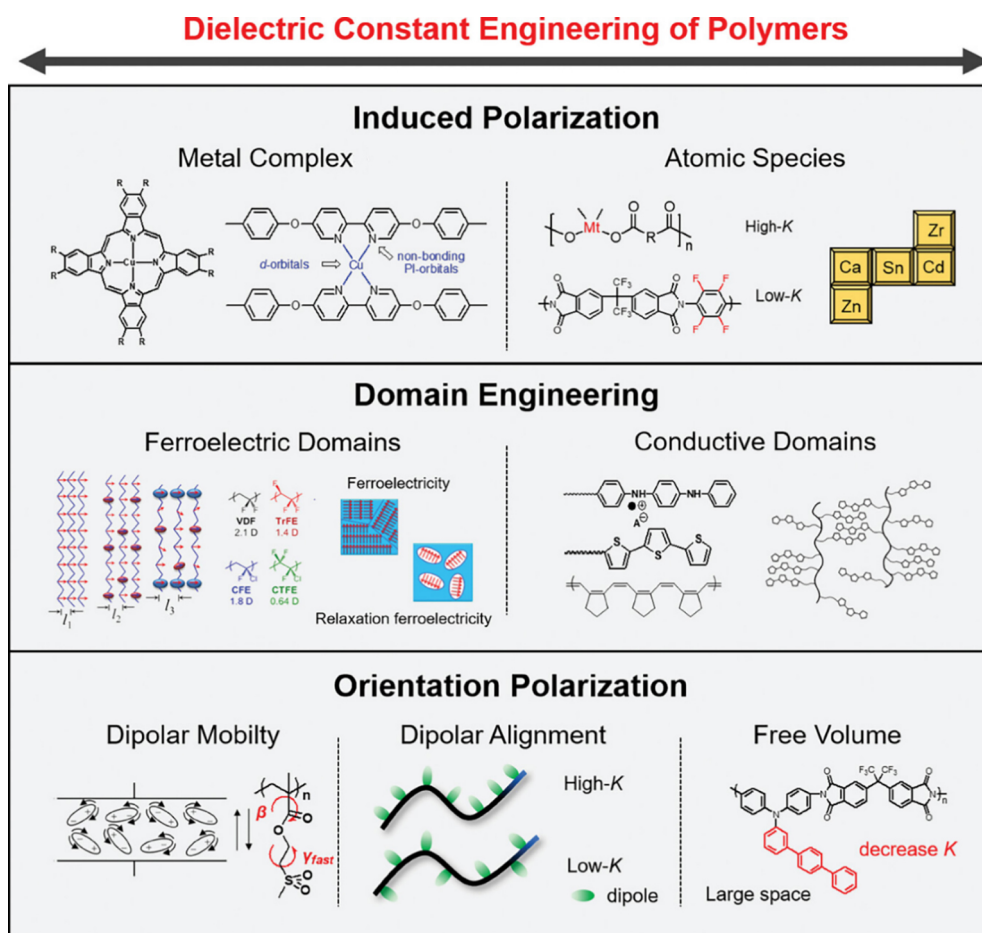
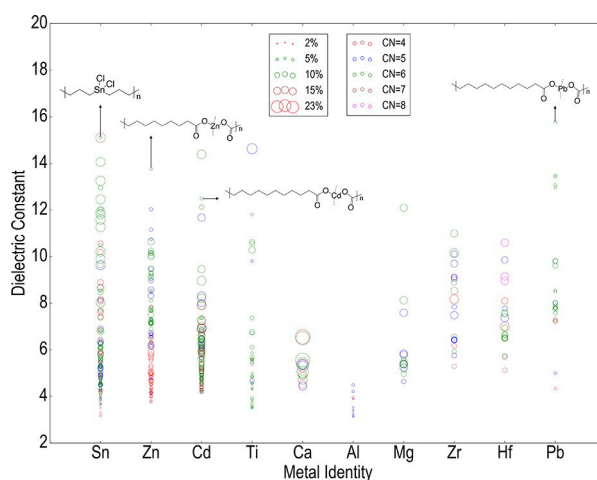


Figure 4. Schematic representation of various polarizations: (A) Electronic polarization; (B) Ionic polarization; (C) Depolarization; and (D) Interfacial polarization^[23].

the nucleus, results in a diminished influence of the nucleus over charge distribution, thereby enhancing the atom's polarizability. As shown in Figure 6, the incorporation of transition metal atoms into a polymer chain via covalent bonding significantly modifies the dielectric constant of the polymer, enhancing its electrical properties and potential applications.

Polarization orientation regulation

Figure 5. Engineering strategy for building dielectric materials^[28].Figure 6. Correlation between ϵ_r and metal properties such as identity, volume fraction and coordination number^[30].

Orientational polarization, a key dipole polarization mechanism, describes the alignment of permanent dipoles in polar polymers under an electric field. While Fröhlich-Kirkwood theory models this behavior well for small rotating molecules, it fails for polymer chains due to dipole interactions, steric effects, and

chain flexibility [Figure 7]^[31]. These constraints reduce ϵ_r by limiting dipole rotation. Engineering dipole mobility and free volume can optimize this polarization in polymers.

Domain engineering

Polymeric materials often contain heterogeneous domains with distinct properties, affecting crystallinity and phase separation. These domains create unique dielectric behavior, with domain relaxation causing time/temperature-dependent ϵ_r variations^[32-33]. Conductive domains form interfaces with the insulating matrix under electric fields, generating Maxwell-Wagner-Sillars polarization that enhances ϵ_r . However, they also increase dielectric loss and reduce E_b via electron tunneling^[34]. Encapsulating conductive domains in insulating polymers reduces leakage while maintaining high ϵ_r , improving overall dielectric performance [Figure 8]^[35].

Energy storage density and storage efficiency

The mechanism of energy storage and release in dielectric materials can be illustrated using a displacement (D)-electric field (E) loop, as depicted in Figure 9. Upon the application of an external electric field, the dielectric material undergoes polarization resulting from the relative displacement of opposing charges within the dipole structure. Following electric field removal, depolarization occurs. This involves the convergence of opposite charge centers. The definite integral of the D-E loop represents the energy density stored during polarization (U_c), as well as the U_d and the η , all of which exhibit temperature dependence. The performance of dielectric energy storage systems is critically dependent on key parameters. These include the slope, maximum electric field strength, and thermal stability of the D-E hysteresis loop.

The polarization state of the dielectric is quantified by the D

$$D = \epsilon_0 \epsilon_r E = \epsilon_0 E + P \quad (3)$$

where E is the applied electric field and ϵ_0 is the dielectric constant of the vacuum (8.854×10^{-12} F/m). Parametric polarization (P) is defined as the total electric dipole moment per unit volume, serving as a metric for assessing the polarization process within the dielectric material. Upon removal of the electric field, a depolarization process ensues, during which the opposing surface charges within the dielectric partially revert to their initial positions. This phenomenon results in a reduction of the D and a decrease in residual polarization. As a result, electrical energy is stored within the dielectric material as electrostatic energy via polarization. This energy is subsequently released during the depolarization process. This mechanism underlies the charging and discharging cycles characteristic of electrostatic capacitors.

Specifically, the dielectric D-E curves for polarization and depolarization processes do not align. This misalignment arises from energy dissipation within the dielectric material, leading to hysteresis loops [Figure 9]. The U_c is calculated by integrating the D with respect to the E along the polarization segment of the D-E loop. Conversely, the U_d is derived from the corresponding integrals along the depolarization segment, as outlined below:

$$U_c = \int_0^{D_{\max}} D dE \quad (4)$$

$$U_d = \int_{D_{\max}}^0 D dE \quad (5)$$

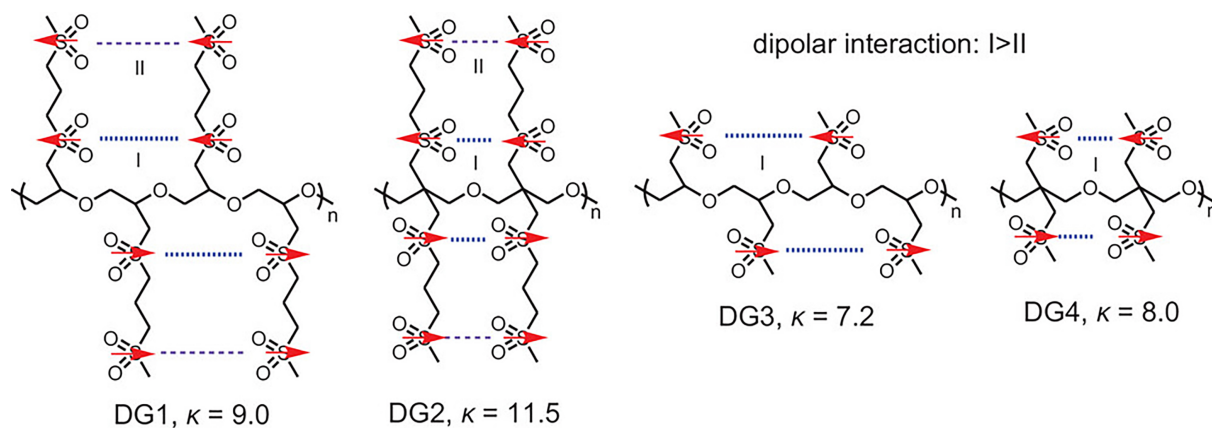


Figure 7. Localized chain conformations (I and II) of compounds DG1-DG4 with different dipole-dipole interactions. Red arrows indicate sulfonyl dipoles. β -leap is attributed to the rotation of the sulfonyl side group [31]. DG: Dipolar glass.

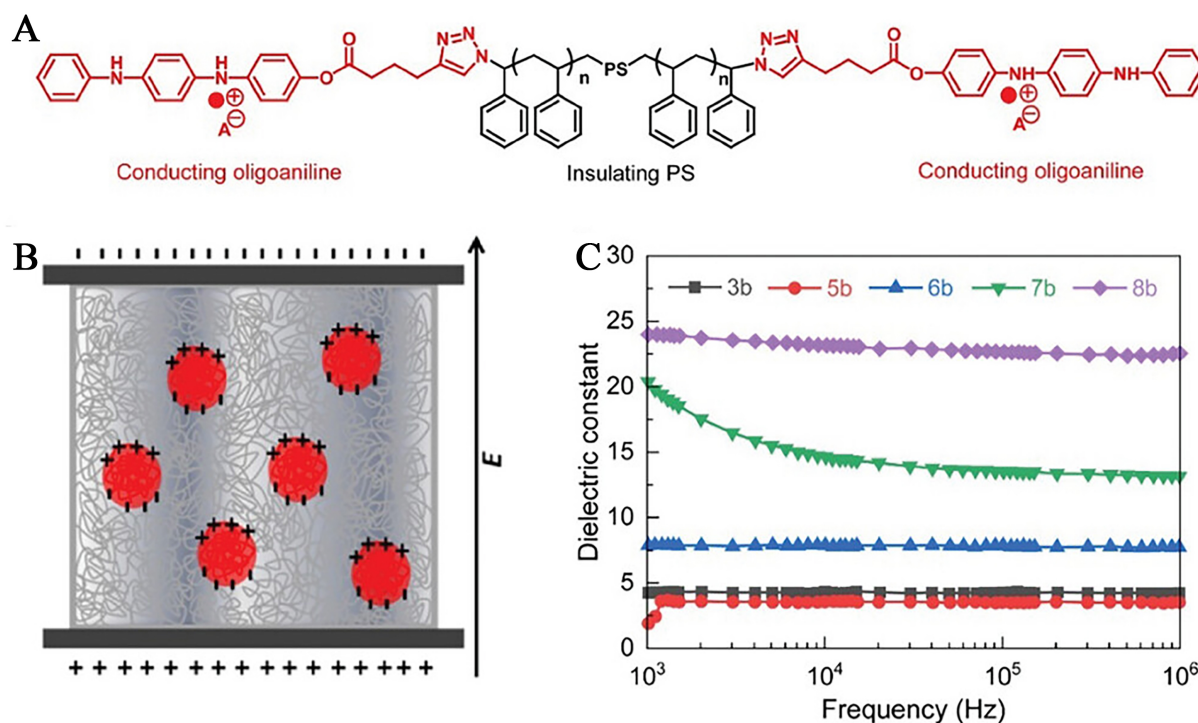


Figure 8. (A and B) Microphase-separated block copolymers including electrically insulating PS matrix and dispersed conductive domains formed by polymer chain segment-oligoaniline ion interactions; (C) Dielectric constants of copolymers with different block structures [36]. PS: Polystyrene.

Furthermore, the energy consumed during the charge-discharge cycle can be quantified by calculating the area enclosed within the dielectric D-E loop. To evaluate the effectiveness of the dielectric material in storing electrical energy while minimizing energy losses, the η is defined as:

$$\eta = \frac{U_d}{U_c} \quad (6)$$

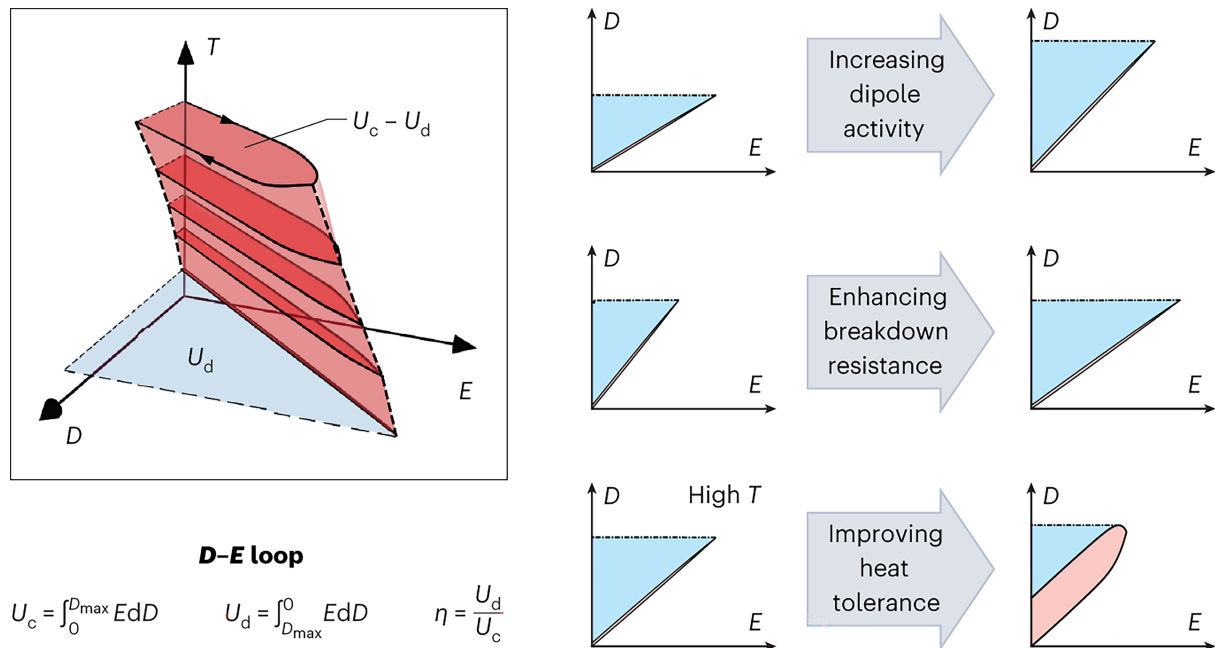


Figure 9. Key characteristics for achieving high energy density in polymer dielectrics^[37]. D-E: Displacement-electric field; U_c : charging energy density; U_d : discharge energy density.

Based on the aforementioned equation, it is evident that when subjected to the combined influences of elevated temperature and high electric field strength, the proportion of energy wasted increases significantly. This condition leads to a reduction in the dielectric material's high voltage resistance, which in turn causes an expansion of the dielectric D-E loop and a decrease in the E_b . Therefore, the thermal stability of the charge and discharge characteristics emerges as a crucial factor in the development of high-performance dielectric materials.

Power density

Moreover, pulsed charge-discharge performance is crucial for dielectric energy storage applications. Optimal power density (P_d) and rapid discharge times ($t_{0.9}$) are essential. In this context, $t_{0.9}$ denotes the duration required to achieve 90% of the final discharge voltage. P_d and current density (C_d) are computed using the equations provided below.

$$P_d = \frac{E \cdot I_{\max}}{2S} \quad (7)$$

$$C_d = \frac{I_{\max}}{S} \quad (8)$$

where S represents the surface area of the electrode, while I_{\max} indicates the maximum current in the underdamped discharge curve at an E . The correlation between U_d and P_d for widely utilized energy storage devices is illustrated in [Figure 10](#).

Recent advances and bottlenecks in composite dielectrics

In prior studies involving polymer nanocomposites, the integration of nanoscale organic and inorganic reinforcements effectively reduced conduction losses and prevented thermal runaway phenomena that occur at elevated temperatures. We have provided a comprehensive summary of the advances achieved in recent years regarding polymer nanocomposites. This summary focuses on key parameters, including ϵ_r , E_b ,

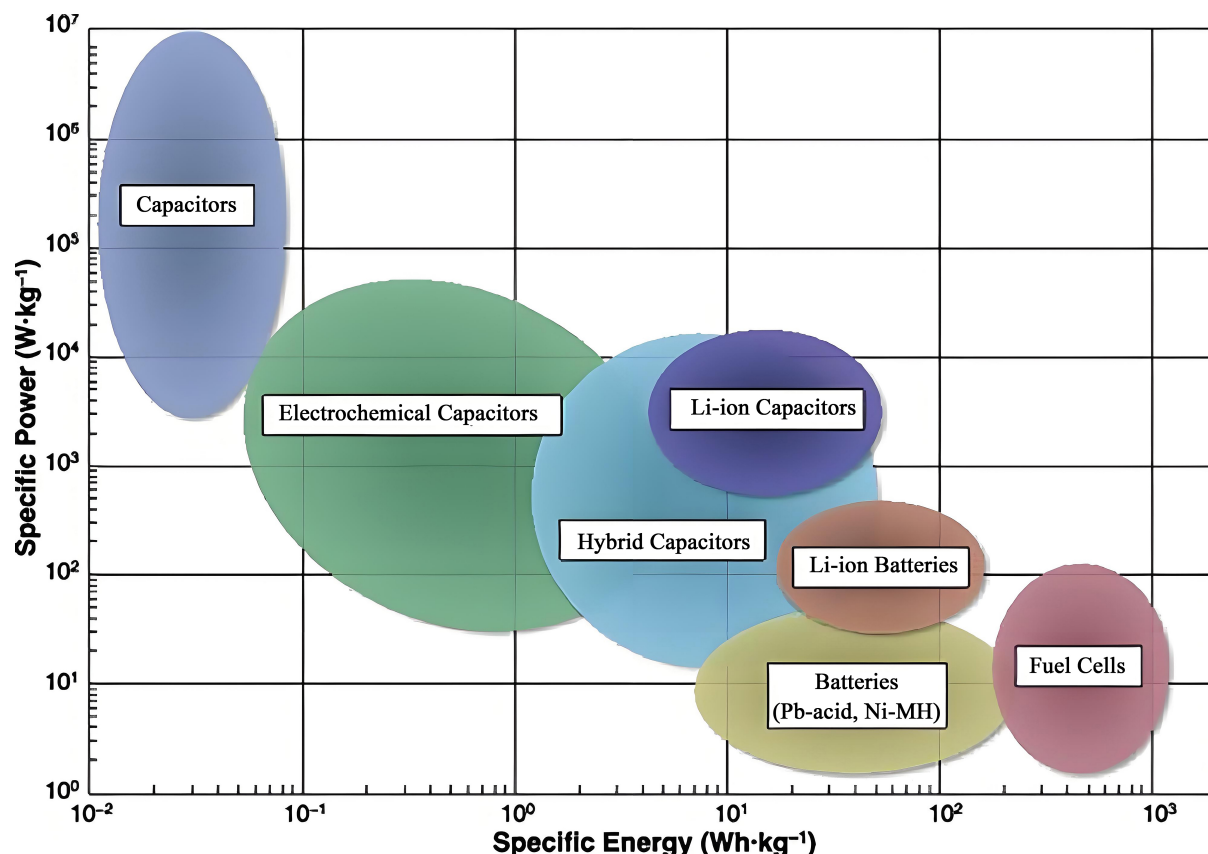


Figure 10. Relationship between energy density and power density of common energy storage devices^[38].

U_e , normalized energy density $W = U_e/E_b$ and η , as presented in Table 1.

Analysis of Table 1 reveals significant variations in ϵ_r across material systems (3.02 to 84.35), with barium strontium titanate-titanium dioxide/polyvinylidene fluoride (BST@TiO/PVDF) achieving maximum ϵ_r through BST/TiO₂ incorporation. E_b enhancements [up to 697.3 MV/m for polyethersulfone-polyetherimides (PES-PEI)] result from innovative fillers, structural optimization, and improved processing. Energy density ranges from 3.19 to 118.65 J/cm³, generally correlating with ϵ_r/E_b , though interfacial/microstructural factors also contribute. Most materials maintain $\eta > 50\%$, with top performers like carboxylated polyarylene ether nitrile@strontium barium titanate nanorod/polyarylene ether nitrile (CPEN@BSTNR/PEN) reaching 95%. The dielectric performance strongly depends on polymer matrix [polyvinylidene fluoride (PVDF), polyetherimide (PEI), *etc.*] and filler [barium strontium titanate (BT), boron nitride nanosheets (BNNs), *etc.*] combinations.

Nevertheless, the intrinsic limitation related to the thermal stability of the host polymer persists as an unresolved issue, thereby impeding advancements in energy storage performance at elevated temperatures. It is well-established that the molecular structure of polymers alters when nearing a solid surface. This results in altered kinetics and a unique glass transition temperature (T_g) for ultrathin polymer films adsorbed on solid surfaces compared to the native polymer^[69–70], with polymer films with free surfaces showing a decrease in T_g ^[71], however, when the surface of the polymer film is wetted, T_g increases due to confinement effects^[72]. Elevated temperatures induce a significant reduction in the polymer's E_b , thereby diminishing energy storage capabilities. This deterioration stems primarily from increased conduction

Table 1. The progress made in recent years in the research of polymer nanocomposites in terms of dielectric constant

	Material system	ϵ_r	E_b (MV/m)	U_e (J/cm ³)	W (kC/m ²)	η (%)	References
1	BT@TOs/PVDF	12.6@1kHz	561.2	21.3	37.95	64	[39]
2	BNNs/P(VDF-HFP)	15.3@10kHz	492	21	42.68	80.2	[40]
3	MF/PVDF _{P&H-x}	15.3@1 kHz	617.1	28.9	46.83		[41]
4	PVDF/f-BSTZT/f ₁ -CNT	41.5@100Hz		14		89.6	[42]
5	CPEN@BSTNR/PEN	17.30@1kHz	204.1	3.19	15.63	95	[43]
6	PEI-PEI/P(VDF-HFP)-P(VDF-HFP)	4.5@100Hz	413	18.9	45.76	90.2	[44]
7	BT-BN/PVDF	35.3@1kHz	500.3	16.1		57	[45]
8	Graphene@TiO ₂ /P(VDF-HFP)	7.44@10kHz	655	19.39	29.60	83	[46]
9	P-30vol.%M/P-M		400	14.86	37.15	94.14	[47]
10	BT@ZIF-67/P(VDF-HFP)	15.3@100Hz	400	12.8	32		[48]
11	TO nb@SO/PVDF	11@100Hz	381.3	8.86	23.24	66.28	[49]
12	BT@MgO/P(VDF-HFP)	11.1@1kHz	423.5	5.6	13.22	51.3	[50]
13	SBN/DPAES/SBT	4.51@1kHz	500	4.64	9.28	84	[51]
14	BNNs-F/PEI		589	5.73	9.73	91.22	[52]
15	BT@TO NPs/PP	3.02@100kHz	580	5.58	9.62	99.3	[53]
16	BST@TiO ₂ /PVDF	84.35@100Hz	29.37				[54]
17	BT@PBCN/PVDF	8.8@1kHz	464	10.86	23.41		[55]
18	C@HTO@AO/PVDF	59.5@100Hz	200.5				[56]
19	BFO@TO-P(VDF-HFP)/PMMA	11.7@1kHz	549.2	19.3	35.14	61	[57]
20	EP/BT@TiO ₂ @PDA-RB		45.7				[58]
21	PVDF/Ta-Al@TiO ₂ NPs/BT	28.2@1kHz	370	16.9	45.68		[59]
22	AZO-BT/PVDF	14.4@1kHz	460	9.1	19.78	57.6	[60]
23	BT@TiO ₂ @SiO ₂ /PVDF	9.4@1kHz	620	19.7	31.77	57.6	[61]
24	SPEN@BTNR/PE	17.1@1KHz	204.8	3.36	16.41		[62]
25	P(VDF-HFP)/P(VDF-TrFE)		694.8	23.6	33.97		[63]
26	Al ₂ O ₃ -PESU	5.0@10Hz	640	8.4	13.13	62	[64]
27	h-BN/PVDF	9.7@1kHz	510	19.256	37.76	52.2	[65]
28	PES-PEI	3.2@1kHz	697.3	6.4	9.18	82.7	[66]
29	O-MMT@TiO ₂ /MVSR	10.28@10Hz	80.21	0.118	1.48		[67]
30	BT NFs/P(VDF-CTFE)	15@100Hz	530	17.1	32.26	84.6	[68]

ϵ_r : Dielectric constant; η : charge/discharge efficiency; E_b : electrochemical breakdown; U_e : energy storage density; BT@TOs: barium strontium titanite nanoparticle@titanium dioxide; PVDF: poly(vinylidene fluoride); BNNs: boron nitride nanosheets; P(VDF-HFP): polyvinylidene fluoride hexafluoropropylene; MF: metal-organic framework-derived Fe; PVDFP&H-x: poly(vinylidene fluoride)Press&Heat-x; f-BSTZT: PVDF/Ba_{0.7}Sr_{0.3}Zr_{0.02}Ti_{0.98}O₃; f₁-CNT: functionalized carbon nanotubes; CPEN: carboxylated polyarylene ether nitrile; BSTNR: strontium barium titanate nanorod; PEN: polyarylene ether nitrile; PEI: polyetherimide; P(VDF-TrFE): poly(vinylidene fluoride-trifluoroethylene); P-30vol.%M/P-M: poly(vinylidene fluoride-hexafluoropropylene)-30 volume percent poly(styrene-methyl methacrylate)/Poly(styrene-methyl methacrylate) composite; ZIF-67: zeolitic imidazolate framework-67; TO nb: titanium dioxide nanobelts; SiO₂: silica; MgO: magnesium oxide; SBN: strontium bismuth niobate; DPAES: diphenylacetylene-endcapped polyarylether sulfone; SBT: strontium barium titanate; BNNs-F: fluorinated boron nitride nanosheets; TiO₂ NPs: titanium dioxide nanoparticles; PP: polypropylene; BST: barium strontium titanite; PBCN: poly[bis(4-cyanophenyl)-2-vinylterephthalate]; C@HTO@AO: amorphous carbon@heterojunction titanium dioxide@aluminum oxide; BFO@TO: bismuth ferrite@titanium dioxide; PMMA: poly(methyl methacrylate); EP: epoxy resin; PDA-RB: polydopamine-randomly dispersed boron nitride nanosheets; Ta-Al@TiO₂ nps: tantalum-aluminum codoped titanium dioxide nanoparticles; AZO-BT: aluminum-doped zinc oxide-barium titanate; SPEN: sulfonated poly(arylene ether nitrile); BTNR: barium titanate nanorods; PE: poly(arylene ether nitrile); PVDF-TrFE: poly(vinylidene fluoride-trifluoroethylene); PESU: polyethersulfone; h-BN: hexagonal boron nitride; PES: polyethersulfone; O-MMT: organically modified montmorillonite; MVSR: methyl vinyl silicone rubber NF: nanofiber; P(VDF-CTFE): poly(vinylidene fluoride-chlorotrifluoroethylene).

nonlinearity resulting from combined thermal and electric field effects. Consequently, mitigating the high-temperature, high-field conduction in polymer dielectrics presents a fundamental challenge.

The intrinsic thermal instability of polymer matrices remains a key limitation for high-temperature energy storage performance. Near solid surfaces, polymer molecular structures reorganize, causing ultrathin films to exhibit modified kinetics and glass transition temperatures (T_g): free-surface films show decreased T_g , while confined/wetted films display increased T_g ^[69-72]. High temperatures severely reduce polymer E_b due to thermally enhanced conduction nonlinearity under electric fields, making conduction suppression a critical challenge.

To address these challenges, the initial step involves ensuring that polymer dielectrics can endure elevated temperatures and pressures. Consequently, polymers exhibiting high T_g or melting temperatures (T_m) have been selected and are commonly utilized in extreme environments^[73-75]. However, their high conductivity limits energy storage performance^[8]. Recent solutions include: (1) Developing wide-bandgap (E_g) polymers by disrupting conjugated backbones, though this requires complex synthesis and reduces thermal stability^[76-77]; (2) Applying insulating coatings to suppress carrier injection^[78-80]. It is crucial to recognize that interfacial adhesion is critical for multilayer films, while inorganic layers may impact self-clearing properties essential for capacitor durability^[81].

High-temperature conduction can be suppressed by carrier traps, achievable through polymer structural modification, inorganic/polymer composites, or all-organic composites. While deeper traps generally enhance energy storage, they may distort local E_s and reduce E_b . Consequently, there is an urgent requirement for quantitative studies to evaluate the impact of trap parameters, including depth, density, and spatial distribution, on the energy storage properties of polymers^[82]. Furthermore, nano-confinement in ultrathin films shows promise for thermal stability, but scalable nanolaminate production via spin-coating/atomic layer deposition (ALD) remains challenging^[83].

High-temperature environments severely degrade polymer dielectrics, causing E_b deterioration, leakage current surges, and significant conduction losses that impair insulation and U_c . Enhancing high-temperature E_b and η requires an in-depth study of nanofiller-polymer interfaces, particularly their polarization mechanisms, charge transfer processes, and thermal stability issues like thermal stress and expansion mismatches, as high temperatures can disrupt interface bonds and intensify molecular chain movement. Recent progress includes experimental approaches like organic-coated nanofillers and heterostructures for interface control^[84], along with theoretical methods such as phase-field breakdown simulations and high-throughput design of laminated dielectrics^[85], all aimed at reducing ferroelectric/dielectric losses while improving high-temperature performance.

Advances in structural designs for high-temperature composite dielectrics

Research on polymers intended for high-temperature dielectric applications has primarily concentrated on enhancing thermal stability, exemplified by elevated glass transition temperatures (T_g), and improving dielectric properties, such as increased ϵ_r . Improvements have been made in the following three ways:

System selection

Table 2 provides a comprehensive summary of the physical properties associated with selected high-temperature polymer dielectrics. Based on their thermal and electrical characteristics, polyimides (PIs), polyetherimides (PEIs), and fluorinated polyimides (FPEs) are the most promising candidates. The aromatic and bulky heterocyclic structures in these polymers contribute to their excellent high-temperature stability^[8].

Table 2. Properties of representative high-temperature polymer dielectrics^[86]

Dielectric	T _g (°C)	ε _r	tan δ	E _b (MV/m) (thickness)	λ (W/m K)
PET	75	3.3	0.005	300 (25 μm)	0.15
PEN	120	3.2	0.005	160 (75 μm)	0.15
PPS	120	3.2	0.002	490 (9 μm)	0.30
PEEK	150	3.1	0.004	200 (50 μm)	0.32
PC	150-210	3.2	0.002	500 (10 μm)	0.21
PESU	225	3.5	0.001	180 (25 μm)	0.18
PEI	217-260	3.2	0.001	200 (25 μm)	0.22
FPE	330	2.8-3.2	0.006	430 (8 μm)	0.20
PI	360-410	3.4-3.5	0.002	300 (25 μm)	0.12
c-BCB	> 350	2.75	0.001	300 (10 μm)	0.30

tan δ: Dissipation factor; PET: polyester; PEN: poly (ethylene glycol naphthalate); PPS: polyphenylene sulfide; PEEK: polyether ether ketone; PC: polycarbonate; PESU: polyethersulfone; PEI: polyetherimide; FPE: fluorene polyester; PI: polyimide; c-BCB: crosslinked divinyltetramethyldisiloxane-bis(benzocyclobutene)

PI, which is a thermosetting material, is synthesized through the polycondensation and subsequent imidization of dianhydride and diamine monomers [Figure 11A]. The inherent imide and aromatic structures in the PI backbone confer exceptional heat resistance, evidenced by a high T_g ranging from 360-410 °C, along with excellent chemical resistance and mechanical strength^[87]. At ambient temperature, PI demonstrates a ε_r of 3.4 and a dissipation factor of 0.002. However, significant increases in conductive losses at high temperatures and electric fields severely limit its energy storage performance. At a temperature of 150 °C and an E_b of 300 MV/m, the η is limited to 15%. Consequently, 85% of the stored energy is lost as Joule heat, yielding a low U_c of 0.36 J/cm³^[88]. These findings demonstrate that despite its high thermal stability, the practical operating temperature of PI is ultimately constrained by increased conductivity at elevated temperatures and electric fields. Therefore, for high-temperature polymer dielectrics, suppressing conductivity is more critical than simply maximizing T_g.

PEI, a PI derivative with main-chain ether bonds (-O-) [Figure 11B], offers improved processability (melt-extrusion/solution-casting) despite lower thermal stability (T_g = 217-260 °C). It delivers superior high-temperature performance: U_c = 1.14 J/cm³ with η = 82% at 150 °C/300 MV/m^[88]. FPE [Figure 11C], synthesized from fluorine bisphenol and phthaloyl chloride, shows exceptional thermal stability (T_g = 330 °C, ε_r stable to 300 °C) with U_c = 1.04 J/cm³ (η = 58%) at 150 °C/300 MV/m^[86]. Its modified version FDAPE (4,9-dialkyl substitution) [Figure 11D] exhibits enhanced T_g = 450 °C while maintaining ε_r = 3.5 and tan δ = 0.003-0.004 from 25-350 °C, making it ideal for wide-temperature power electronics^[89].

Packing selection

To enhance high-temperature energy storage in dielectric polymers, polymer nanocomposites with nanoscale reinforcements have been developed. Inorganic nanofillers (e.g., BN, Al₂O₃) with high thermal conductivity and wide bandgaps improve heat dissipation and high-temperature electrical insulation. Alternatively, all-organic nanocomposites reduce conductivity and stabilize charge transfer using high electron-affinity molecular fillers or blends.

Inorganic fillers

Nanofillers with wide bandgap

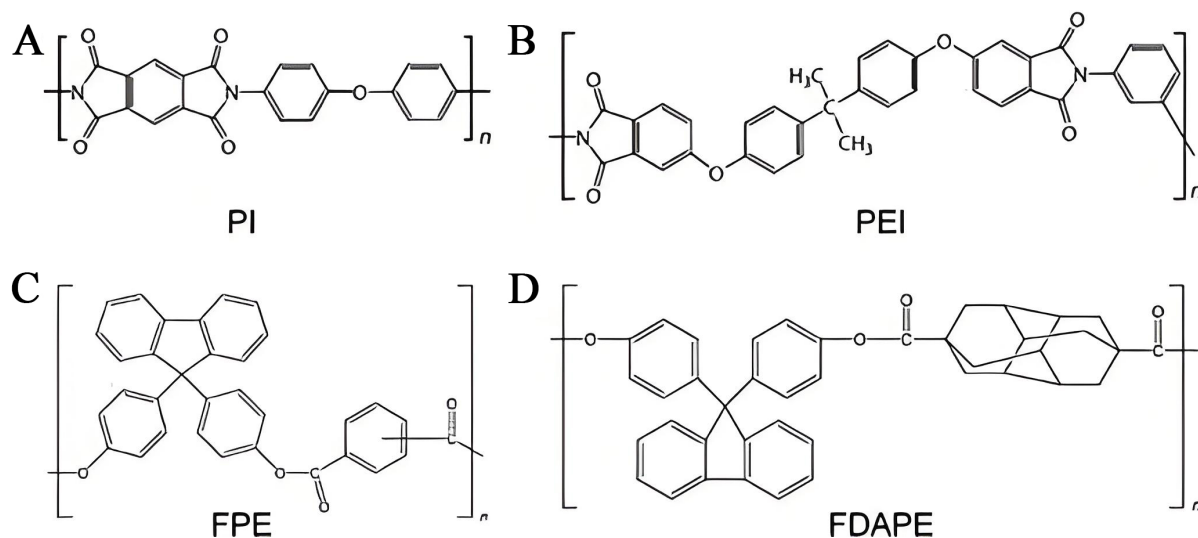


Figure 11. Chemical structures of (A) PI; (B) PEI; (C) FPE; and (D) fluorene-based polyesters with 4,9-diamantane groups ^[87]. PI: Polyimide; PEI: polyetherimide; FPE: fluorene polyester; FDAPE: fluorenyl polyester with 4,9-diamantyl group.

To study the room temperature dielectric energy storage, it was found that high dielectric ceramics doped with barium titanate (BaTiO_3), sodium niobate (NaNbO_3), and barium strontium titanate ($\text{Ba}_x\text{Sr}_{1-x}\text{TiO}_3$) can improve the ϵ_r and U_c of polymer matrix^[90–94], but their high-temperature performance remains poor. For instance, PI/BT nanocomposites show improved dielectric stability (up to 200 °C) but low η due to ϵ_r mismatch-induced field distortion, leakage current, and reduced E_b ^[95–96]. Shen *et al.*^[97] developed a phase-field model [Figure 12A–G] showing that Joule heating exponentially degrades E_b in PI/STO films, with filler orientation (perpendicular to field) and reduced conductivity improving thermal stability [Figure 12H]. Before winding, the film's maximum temperature (T_{\max}) is consistent with the ambient temperature. Following capacitor fabrication, however, both T_{\max} and the E_b degradation factor increase, accompanied by elevated dielectric loss [Figure 12I]. Wang *et al.*^[98] found MgO's wide bandgap reduces conductivity loss in PI composites, achieving 4.78 J/cm³ at 433 MV/m and 150 °C, demonstrating filler morphology's critical role in insulating properties and E_b .

Unlike doped high ϵ_r ceramic fillers, the incorporation of wide bandgap nanofillers tends to improve the insulating properties of polymers more efficiently, resulting in superior high-temperature energy storage performance^[99–102]. For example, Li *et al.*^[100] incorporated BNNs (5.97 eV, 300 W/m·K) into BCB, reducing leakage current by 10× and conductivity loss from 18% to 3% at 200 MV/m (10 vol.%). The composite achieved 2 J/cm³ at 150 °C/400 MV/m with $\eta > 90\%$, attributed to BNNs creating deep traps that suppress P–F emission and carrier migration. BNNs also increased thermal conductivity to 1.8 W/m·K, mitigating thermal degradation.

Ai *et al.*^[101] systematically investigated the effects of filler permittivity (ϵ_r) and E_g on nanocomposite properties using Al_2O_3 ($\epsilon_r = 9.5$, $E_g = 8.6$ eV), HfO_2 (25, 5.8 eV), BNNs (4, 5.97 eV), and TiO_2 (110, 3.5 eV) as nanofillers [Figure 13A–C]. The results demonstrated that E_b increased with filler E_g but decreased with higher ϵ_r . At 150 °C, the conductivity loss decreased by 41.1% (TiO_2) to 93.9% (Al_2O_3) compared to pure PI. Wide-bandgap fillers ($\text{Al}_2\text{O}_3/\text{HfO}_2$) not only minimized conductivity loss and achieved the highest η , but also exhibited superior charge trapping capability as confirmed by thermally stimulated depolarization current (TSDC) tests [Figure 13D]. These findings explain why $\text{Al}_2\text{O}_3/\text{HfO}_2$ composites showed significantly better U_d than high- ϵ_r TiO_2 systems.

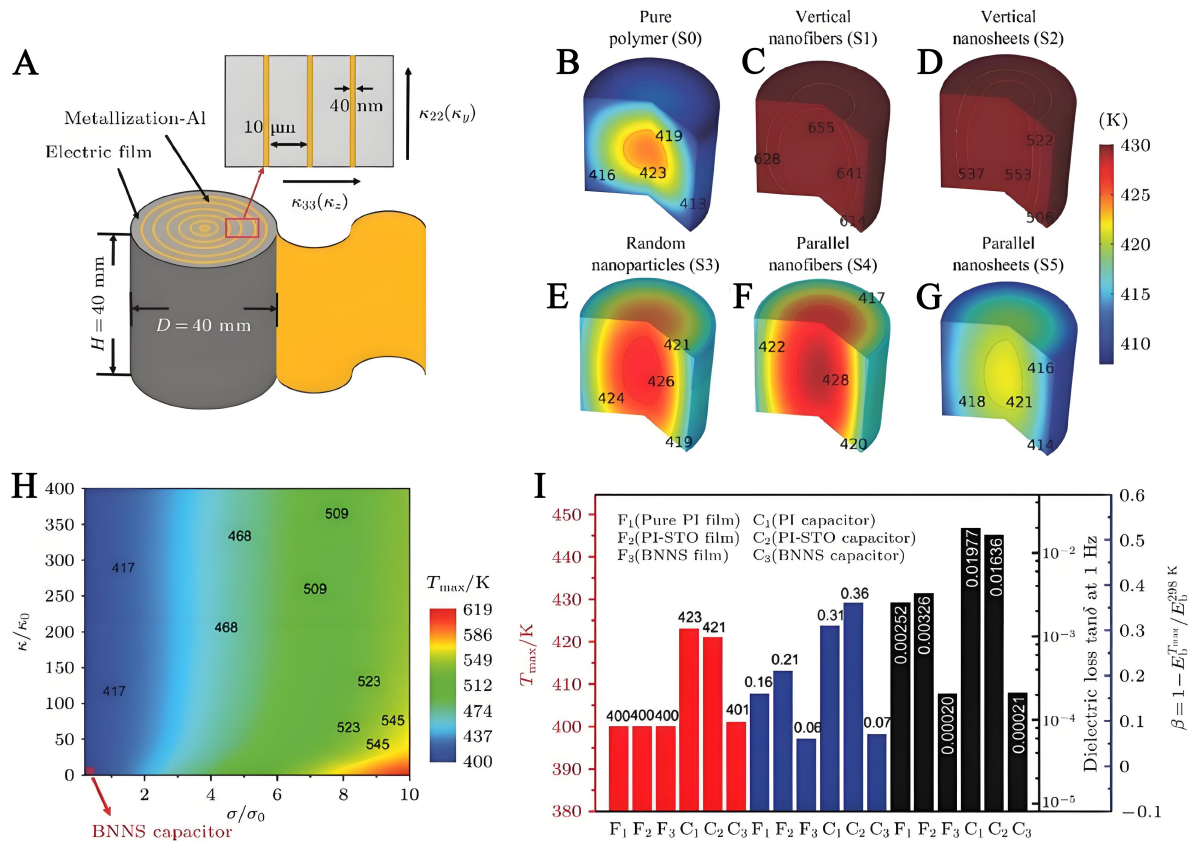


Figure 12. (A) Temperature distribution in PI-STO nanocomposite capacitors at 200 kV/mm and 400 K; (B) Pure PI; (C) Vertical nanofibers; (D) Vertical nanosheets; (E) random nanoparticles; (F) Parallel nanofibers; (G) Parallel nanosheets; (H) T_{max} vs. thermal/electrical conductivity; (I) Performance comparison of T_{max} (red), E_b degradation β (blue), and $\tan \delta$ (black) under six conditions^[97]. PI: Polyimide; STO: polyimide; E_b : electrochemical breakdown; $\tan \delta$: dissipation factor.

High-aspect-ratio Al_2O_3 nanofibers (NWs) and nanosheets (NPLs) outperform nanoparticles (NPs) in enhancing polymer dielectric properties. Li *et al.*^[100] prepared c-BCB/ Al_2O_3 composites showing NPLs' superior E_b (489 MV/m at 150 °C vs. NWs' 385 MV/m and NPs' 334 MV/m). Phase field simulations demonstrated NPLs' greater breakdown resistance by inhibiting breakdown phase growth and providing more uniform electric field distribution compared to NPs/NWs. The wide-bandgap Al_2O_3 NPLs introduced deep traps, reducing leakage current. At 7.5 vol.%, c-BCB/ Al_2O_3 NPLs achieved $U_e = 4.07 \text{ J/cm}^3$ ($\eta = 82\%$) at 150 °C/450 MV/m.

Although wide bandgap nanofillers can significantly reduce the conductivity loss of the polymer matrix at high temperatures and improve the η , the improvement of the ϵ_r and U_e of the composites is still limited. Li *et al.*^[103] combined carbon quantum dots (CQDs) with the diamine monomer of PEI to integrate high electrical insulation and high thermal conductivity. The Coulomb blockade effect of CQDs restricts electron migration, and the bonding network formed by CQDs and PEI deepens and densifies the traps. As a result, compared with pure PEI, the U_d of the hybrid dielectric (PEI-NH₂-CQDs) at 200 °C with a η of 90% is increased by 80%. With the intention of enhancing both dielectric and insulating properties concurrently, Li *et al.*^[8] prepared PEI/BTNPs/BNNs ternary nanocomposites by blending BNNs with high dielectric strength and BT nanoparticles (BTNPs) with high ϵ_r , which have complementary functions. By varying the proportion of BTNPs and BNNs, the high-temperature energy storage performance of the nanocomposites was significantly enhanced. When the volume fractions of BTNPs and BNNs were set at 1.27 vol.% and 6.05

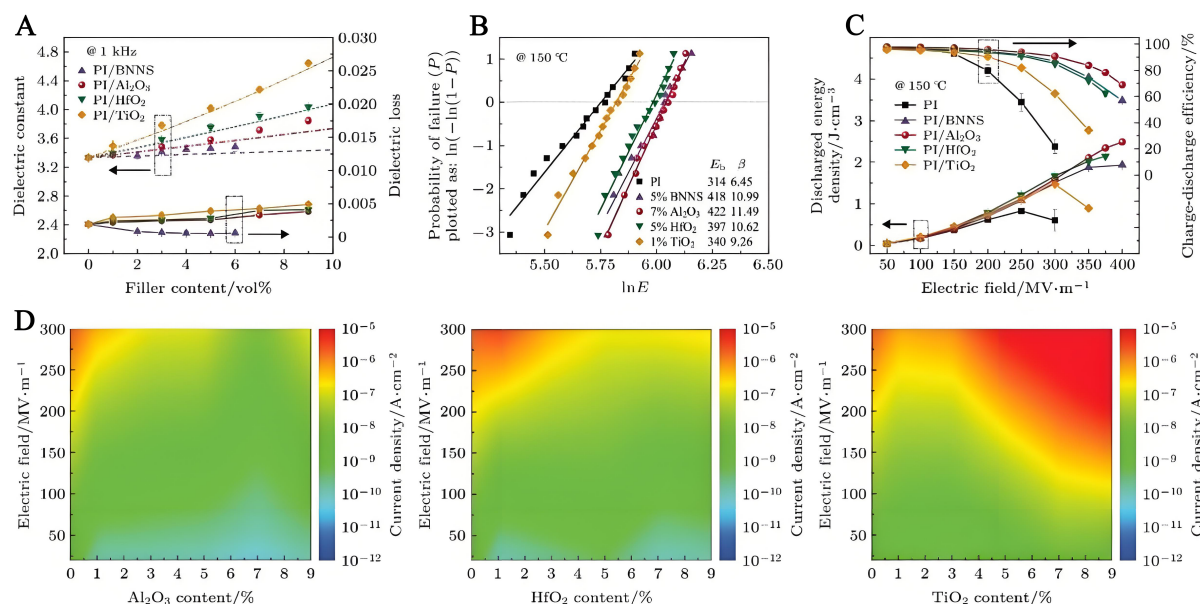


Figure 13. Dielectric and energy storage properties of PI nanocomposites: (A) ϵ_r /loss vs. filler content (25 °C, 1 kHz); (B) Weibull E_b and (C) U_e at 150 °C; (D) Simulated current density vs. filler content/E-field (Al₂O₃/HfO₂/TiO₂, 150 °C)^[101]. PI: Polyimide; ϵ_r : dielectric constant; E_b : electrochemical breakdown; U_e : energy storage density.

vol.%, respectively, the U_e of the resulting nanocomposites at a temperature of 150 °C achieved 2.92 J/cm³. Additionally, the E_b reached 547 MV/m, representing increases of 83% and 25%, respectively, compared to the original PEI material.

Nanofillers with low doping ratio

Unlike previous high volume fraction doping, Thakur *et al.*^[104] demonstrated that ultralow nanoparticle doping (< 0.5 vol.%) enhances ϵ_r through multilayer interfacial polarization, with 20nm Al₂O₃/PEI (0.32 vol.%) achieving $\epsilon_r = 5$ (55% increase) while maintaining low loss, though E_b and η remain unaffected. Yang *et al.*^[105] achieved superior performance using 0.2 wt.% phosphotungstic acid sub-nanosheets in PEI, which trap charges and suppress breakdown, yielding $U_e = 7.2$ J/cm³ at 200 °C with $\eta = 90\%$ and 5×10^5 cycle stability.

Compared to amorphous PEI, semicrystalline/single-crystal polymers exhibit lower conductivity loss owing to their wider E_g ^[106]. Zhang *et al.*^[14] employed high- T_g semicrystalline poly(arylene ether urea) (PEEU) as matrix with 0.21 vol.% nano-Al₂O₃ filler, increasing ϵ_r from 4.7 to 7.4. The Al₂O₃ expanded chain spacing and disrupted hydrogen bonds to enhance dipole response, while simultaneously restricting dipole mobility and elevating trap energy levels, significantly reducing high-field conductivity loss. The PEEU/Al₂O₃ films achieved a discharge energy density of 5 J/cm³ at 150 °C with $\eta > 90\%$. However, low-concentration doping is not universally effective - for instance, 0.5% Al₂O₃ in semicrystalline tetrafluoroethylene hexafluoropropylene vinylidene fluoride (THV) only reduced high-temperature/high-field conductivity loss without markedly improving dielectric properties^[107].

Surface-modified nanofillers

The interfacial structure between organic and inorganic phases significantly influences nanocomposite properties. Inherent physicochemical differences often lead to defects and voids at these interfaces, degrading mechanical and electrical performance^[108]. To enhance interfacial compatibility and performance, researchers have employed surface modification strategies. For example, Xu *et al.*^[109], inspired by spider silk's hierarchical nanostructure, combined long-chain poly(aryl ether sulfone) (DAPES) with BCB-modified BN nanosheets [Figure 14]. This approach enhanced interfacial integrity, achieving $U_e = 2.7 \text{ J/cm}^3$ with $\eta > 90\%$ at $150^\circ\text{C}/400 \text{ MV/m}$. Wang *et al.*^[110] strengthened the surface of polymer composite dielectrics with in-situ generated ultrafine SiO_2 nanoparticles and the bulk phase with commercially available SiO_2 nanoparticles. The E-c- SiO_2 NPs/PEI film showed significantly improved performance. At 200°C and 530 MV/m , its U_d reached 4.26 J/cm^3 , a 1,274.19% increase over the pristine PEI film.

In summary, high-performance polymer nanocomposite dielectrics for high-temperature/high-field applications can be achieved by incorporating optimized inorganic nanofillers, where filler bandgap, size, morphology, distribution, and interfacial structure critically govern U_d and η .

Organic-organic and organic-inorganic nanocomposites

Microstructure design is vital for optimizing organic-organic dielectric nanocomposites. Core-shell and gradient structures, precisely controlled in nanoparticle aspects, can significantly boost dielectric properties. Incorporating high- ϵ_r organic nanoparticles and using multilayer structures help maintain high permittivity and greatly enhance E_b .

In organic-inorganic systems, performance depends on the uniform dispersion or well-controlled alignment of inorganic nanoparticles in the polymer matrix, influenced by inorganic particle surface properties, polymer matrix features, and processing methods. The high permittivity of inorganic fillers offers more design flexibility for advanced dielectric materials.

Both organic-organic and organic-inorganic dielectric nanocomposites are promising for advanced energy storage and electronics. By precisely controlling microstructure with synthesis techniques and understanding mechanisms, customizing materials for specific applications is achievable. Future research should focus on developing new nanofillers, improving interfacial interactions, and exploring new polymer matrices to further enhance nanocomposite dielectric properties.

Specifically, the molecular structure of polymers is not only closely associated with the mechanical properties and thermal stability of polymer materials, but also significantly affects their electrical properties^[111-112]. Unlike nanocomposite dielectric materials, polymeric materials possess an inherent advantage in terms of structural tunability and designability, thereby heralding the emergence of all-polymer materials with superior performance.

Incorporating wide-bandgap fillers via physical blending effectively enhances the E_b and U_d of high-temperature polymers by introducing deep traps that suppress charge transport while maintaining flexibility. Ding *et al.*^[113] blended PEI with PEEU, where unbonded urea groups acted as deep traps to improve E_b . Zhang *et al.*^[114] demonstrated that strong intermolecular interactions in PEI/PI blends reduced internal defects, enhancing E_b . Feng *et al.*^[115] introduced poly(vinylidene fluoride-co-hexafluoropropylene) P(VDF-HFP) into PI, creating interfacial deep traps through phase separation to boost η at high temperatures. Notably, Zhang *et al.*^[116] achieved an E_b of 540 MV/m and U_d of 5.92 J/cm^3 ($\eta > 90\%$) at 150°C in PEI/0.5 wt.% PVDF composites, attributed to nanoscale phase separation. Similarly, Shang *et al.*^[66] fabricated electrospun PEI/polyethersulfone (PES) films with a U_d of 5.28 J/cm^3 ($\eta = 90\%$) at 150°C and

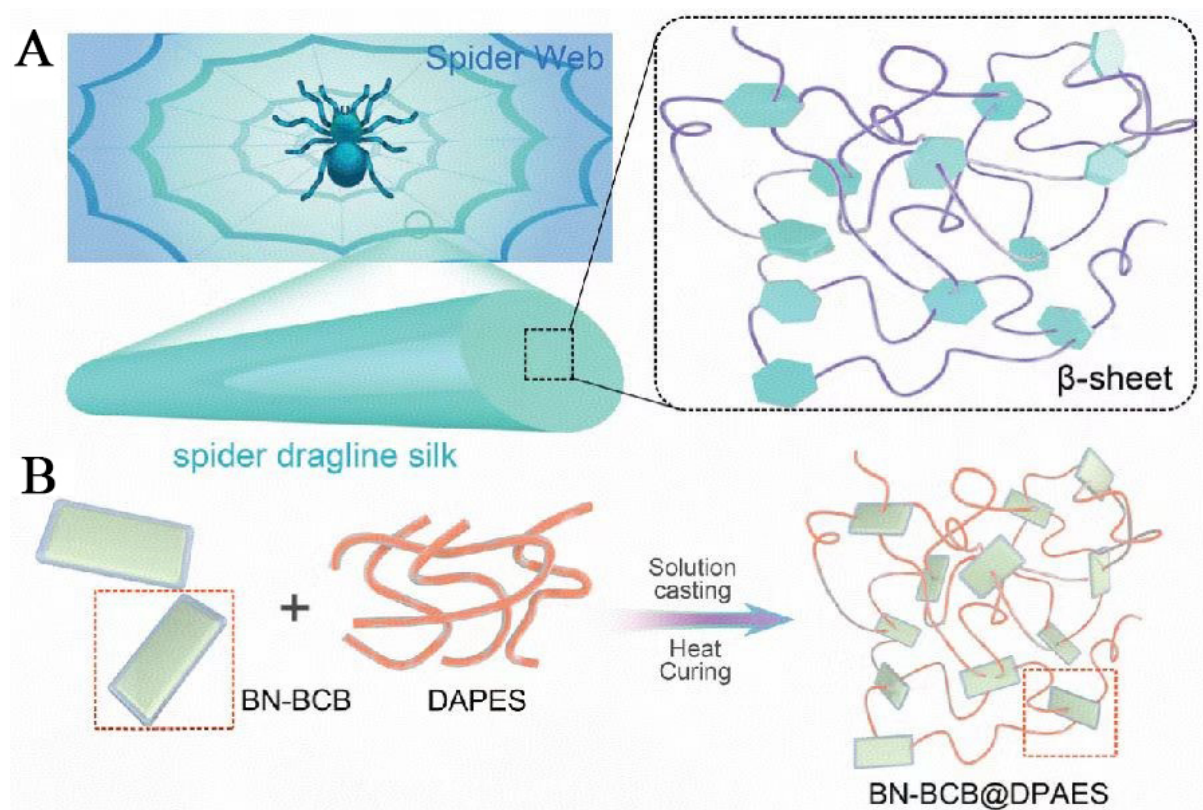


Figure 14. (A) Microstructure of spider silk and spider filaments; (B) Process diagram of BN-BCB@DPAES composites^[109]. BN-BCB: Boron nitride-divinyltetramethyldisiloxane-bis(benzocyclobutene); DPAES: poly(aryl ether sulfone).

excellent cycling stability over 50,000 cycles, outperforming individual components. Xing *et al.*^[117] prepared a nano-submicron structured film composed of P(VDF-HFP) and polymethyl methacrylate (PMMA) through electrospinning. This structure maximizes the utilization of the ferroelectric material components without sacrificing the E_b and η , and achieves improved dielectric properties. The sample reaches a U_d of 13.72 J/cm³ with a η of 80% at 740 kV/mm.

To increase the U_d , the introduction of high-volume fraction fillers encounters the challenge of filler aggregation. Yang *et al.*^[118] developed PEI composites with trace hydroxyapatite (HAP) sub-nanofibers (0.9 nm diameter, Figure 15A and B) modified with oleic acid/octadecylamine. These sub-nanofibers provide large interfacial areas at low concentrations (0.5 wt.%), where surfactants boost dipole polarization via increased free volume while creating charge traps to improve E_b . The HAP/PEI nanocomposites [Figure 15C] achieved U_d of 5.14 J/cm³ (150 °C) and 3.1 J/cm³ (200 °C) with η = 90%, maintaining stability over 3×10^5 cycles. Notably, their 200 °C performance surpassed BOPP's 70 °C capability [Figure 15D].

Small molecule fillers, featuring good polymer compatibility and adjustable structures, boost polymer dielectric energy storage. However, doping above 1 wt.% undermines the polymer matrix's thermal stability. Yang *et al.*^[119] crafted a high-stability bifunctional dipole glass polymer (MW > 30,000 g/mol) using cyclohexane and sulfone functional groups. This enables up to ~10 wt.% doping while maintaining stability. Such a design enhances ϵ_r and E_b by optimizing the free-volume distribution around polar groups. The resultant blend achieves U_d of 8.34 J/cm³ at 150 °C and 6.21 J/cm³ at 200 °C (η = 90%). It also shows stable charge-discharge cycling (50,000 cycles) at 200 °C and 600 MV/m.

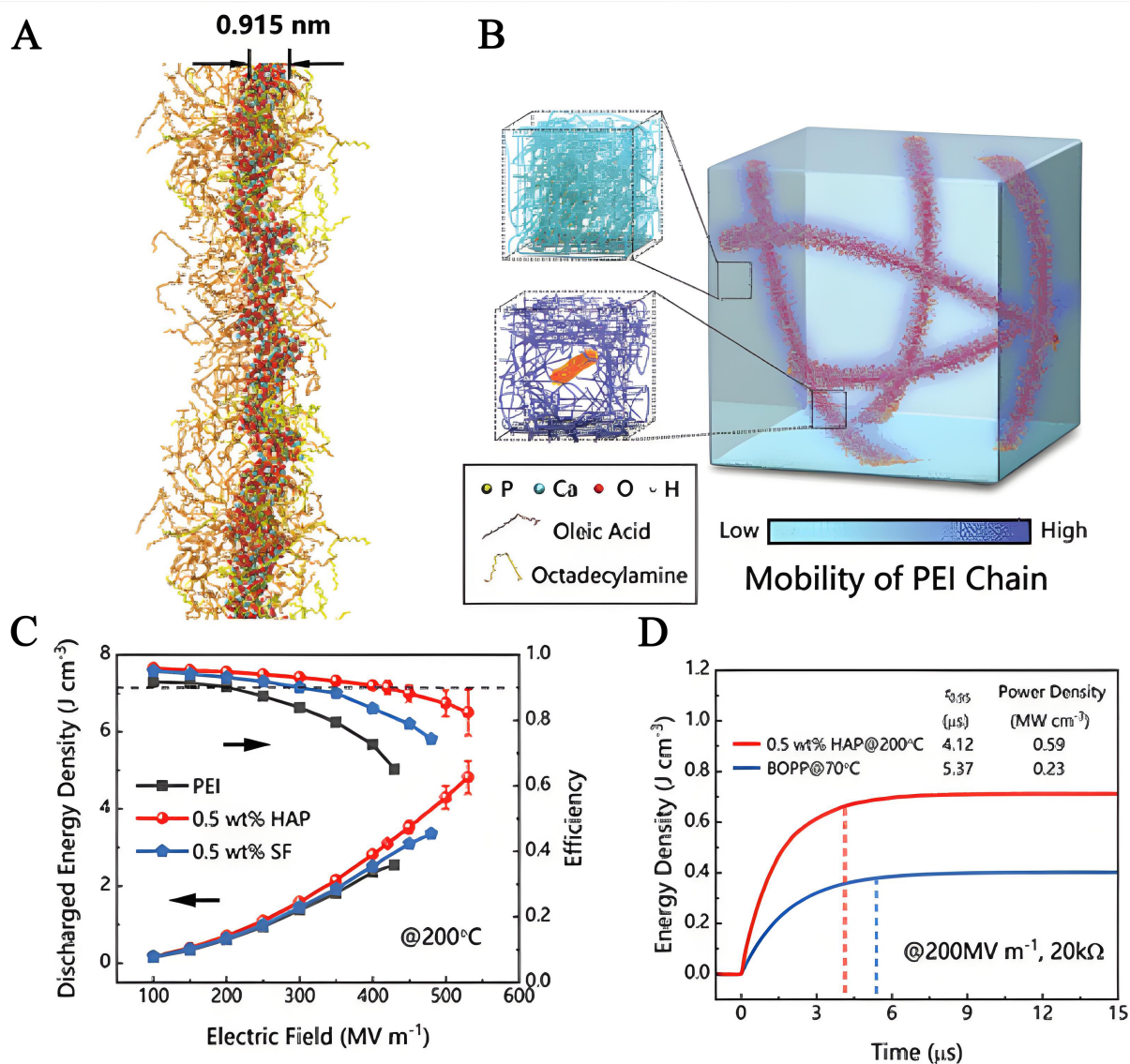


Figure 15. (A) HAP sub-nanofiber structure; (B) PEI-HAP composite with ultra-low filler content, showing chain distribution/mobility in matrix (dense) and interface (loose); (C) U_d and η of PEI, PEI-0.5wt.%HAP, and PEI-0.5wt.%SF at 200 °C vs. electric field; (D) U_e vs. discharge time for PEI-0.5wt.%HAP (200 °C) and BOPP (70 °C)^[118]. HAP: Hydroxyapatite; PEI: polyetherimide; U_d : discharge energy density; η : charge/discharge efficiency; U_e : energy storage density.

Structural configurations

Polymer structural designs, such as bilayer and multilayer structures, can enhance ϵ_r and E_b . In multilayer structures, the large, flat interfaces between alternating phases play a crucial role. They enhance interfacial polarization, which impacts ϵ_r , and redistribute the electric field. The high E_b phase blocks conductive paths, and the high ϵ_r phase improves polarization^[120–121].

Multilayer inorganic/polymer composites significantly enhance capacitive performance through three synergistic mechanisms: interfacial carrier traps, suppressed charge injection, and reduced filler agglomeration. Liu *et al.*^[122] demonstrated this approach by fabricating PI-BNNs bilayer films via layer-by-layer solution casting, where the PI-BNNs interface created deep traps [validated by density functional theory (DFT) and TSDC measurements] that reduced leakage current, achieving exceptional energy storage

performance with $U_d = 4.37 \text{ J/cm}^3$ and $\eta = 92\%$ at 200°C . Extending this strategy, Guo *et al.*^[123] developed sandwich-structured $0.55\text{Bi}_{0.5}(\text{Na}_{0.84}\text{K}_{0.16})_{0.5}\text{TiO}_3\text{-}0.45(\text{Bi}_{0.1}\text{Sr}_{0.85})\text{TiO}_3$ (BNKT-BST)/PEI composites [Figure 16] featuring BNKT-BST ceramic interlayers with remarkable intrinsic properties ($\eta > 98\%$ at breakdown field). This design simultaneously enhanced ϵ_r , E_b , and mechanical properties while reducing dielectric losses. The optimized trilayer 0-0.75-0 structure delivered outstanding performance metrics: a record U_d of 7.7 J/cm^3 with $\eta = 80.2\%$ at 150°C under 650 MV/m , along with excellent cyclic stability maintaining U_d between $4.67\text{-}4.77 \text{ J/cm}^3$ and η exceeding 90% at 500 MV/m , demonstrating the effectiveness of multilayer architectures for high-temperature dielectric applications. Similarly, Zhang *et al.*^[124] designed a three-layer (B-G-B) sandwich-structured dielectric film by alternately spin-coating composite solutions of BN/PMMA and graphene nanosheets (GNS)/PMMA. This structure achieved improved performance through synergistic effects, where the ϵ_r reached 4.3 (@ 1 kHz), and the E_b reached 458.6 kV/mm , which were 119% and 113% higher than those of pure PMMA, respectively.

All-organic polymer composites demonstrate superior flexibility and manufacturability compared to inorganic/polymer systems by eliminating property mismatch issues^[125]. Niu *et al.*^[126] designed PEIs-PI-PEIs sandwich-structured films where PI surface expansion upon contact with PEI solution induces interfacial molecular rearrangement, forming deep trap energy levels. This unique structure significantly reduces high-temperature conductivity, achieving an energy loss of only 0.06 J/cm^3 at $150^\circ\text{C}/250 \text{ MV/m}$ (2.9% of pure PI) while maintaining $\eta > 90\%$ with $U_d = 2.0 \text{ J/cm}^3$ at 200°C . Sun *et al.*^[127] developed bilayer PVDF/PEI films featuring heterogeneous molecular interpenetration interfaces. The interfacial interactions induce polarity phase transformation that increases β/γ -phase content while reducing molecular chain spacing. This simultaneously enhances Young's modulus to alleviate local stress distortion. The optimized film achieves remarkable performance: $U_d = 29.89 \text{ J/cm}^3$ with $\eta = 81.1\%$ at 940 MV/m , and maintains $U_d = 22.89 \text{ J/cm}^3$ when $\eta \geq 90\%$.

Research on high-temperature dielectric polymers focuses on enhancing thermal stability and dielectric properties through material selection, filler optimization, and structural engineering. Promising polymer matrices include PI (high thermal stability but with conductive losses), PEI (excellent processability and high-temperature performance), and modified FPE. For fillers, wide-bandgap nanofillers like Al_2O_3 outperform high ϵ_r ceramics in improving insulation, while low doping ratios ($< 0.5 \text{ vol.}\%$) can enhance ϵ_r in some crystalline polymers. Surface modification improves interfacial compatibility, and tailored microstructures (e.g., sub-nanofibers) further boost performance. Structurally, multilayer/bilayer designs (inorganic-polymer or all-organic) synergistically increase ϵ_r and E_b , with all-organic composites offering scalability advantages.

CONCEPTUAL DESIGN FOR HIGH-TEMPERATURE DIELECTRIC COMPOSITES

Machine learning technique

To accelerate the promotion of composite dielectrics in practical applications, predictive design tools are of great importance, such as density functional theory, molecular dynamics simulation, and machine learning (ML). Among them, ML has become the research focus due to its powerful data analysis capabilities^[128]. In materials science, it is widely applied in various aspects, including material composition design, process optimization, performance prediction, and evaluation. Shen *et al.*^[129] summarized the six steps of the ML workflow, as shown in Figure 17.

The complexity of dielectric properties limits available data. Figure 18 illustrates the use of advanced computational techniques, including numerical simulations, molecular dynamics (MD), and finite element methods, to obtain crucial information^[130]. Most basic dielectric properties can be simply determined or

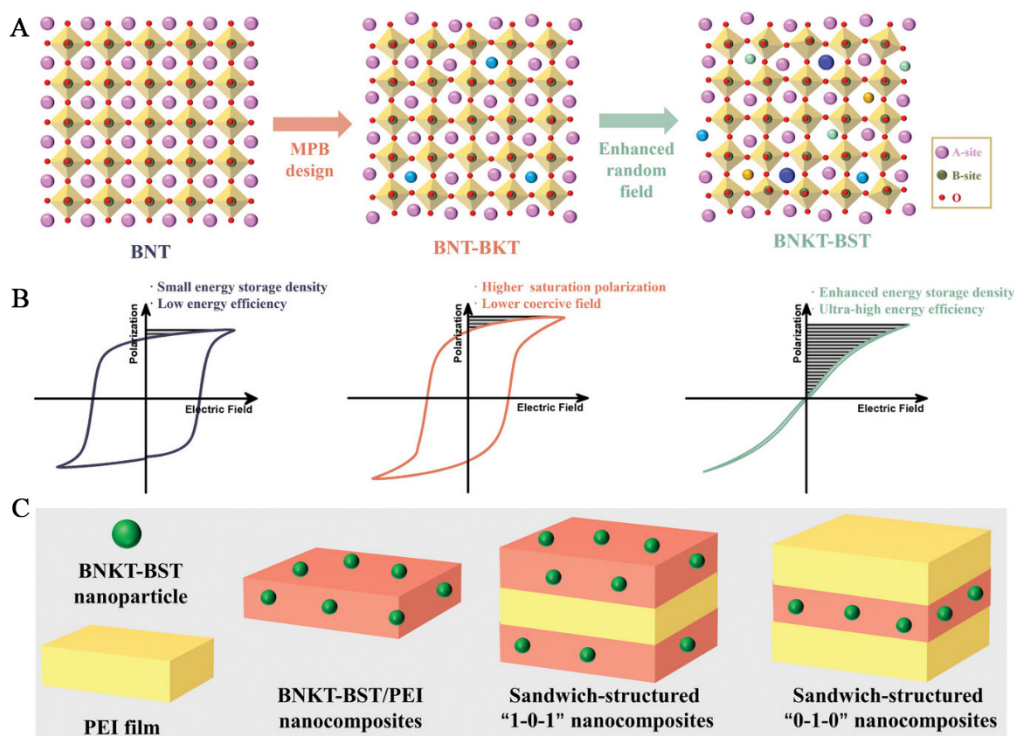


Figure 16. Ultrahigh U_d vs. η in ceramic/polymer composites via stacked design: (A and B) BNT/BNKT/BNKT-BST structure and D-E behavior; (C) BNKT-BST/PEI fabrication process^[123]. BNT: $\text{Bi}_{0.5}\text{Na}_{0.5}\text{TiO}_3$; BNKT-BST: $0.55\text{Bi}_{0.5}(\text{Na}_{0.84}\text{K}_{0.16})_{0.5}\text{TiO}_3-0.45(\text{Bi}_{0.1}\text{Sr}_{0.85})\text{TiO}_3$; PEI: polyetherimide; U_d : discharge energy density; D-E: displacement-electric field.

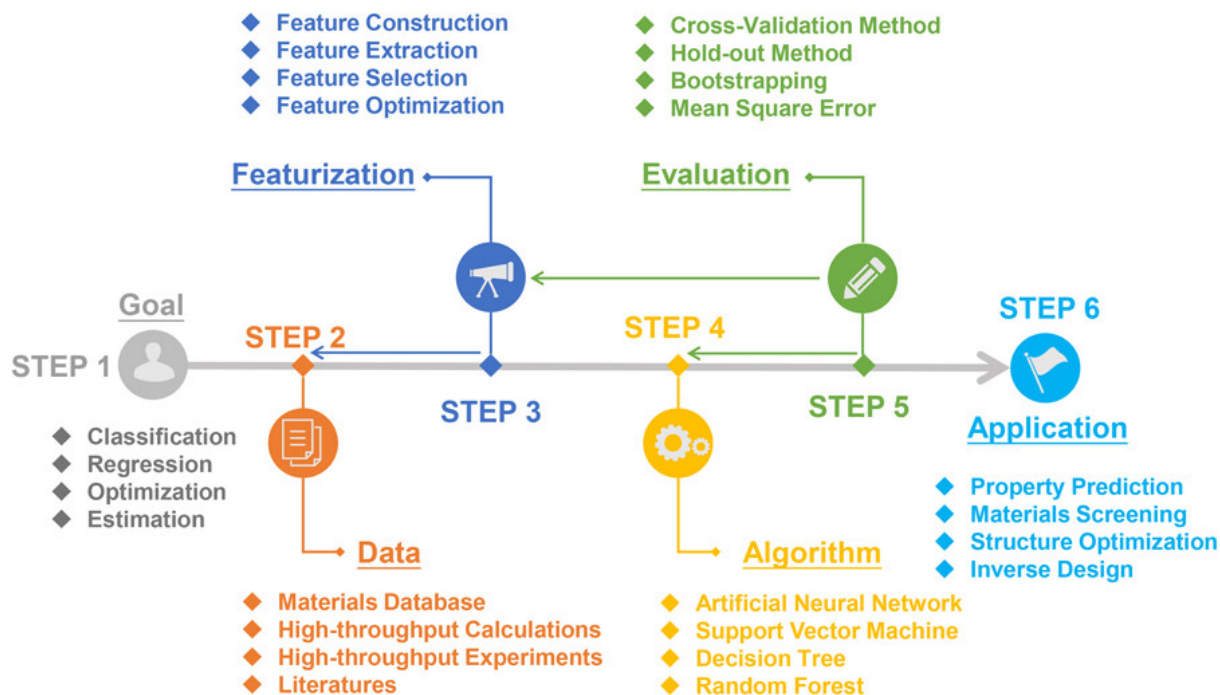


Figure 17. Workflow of a generic ML model with six steps^[129].

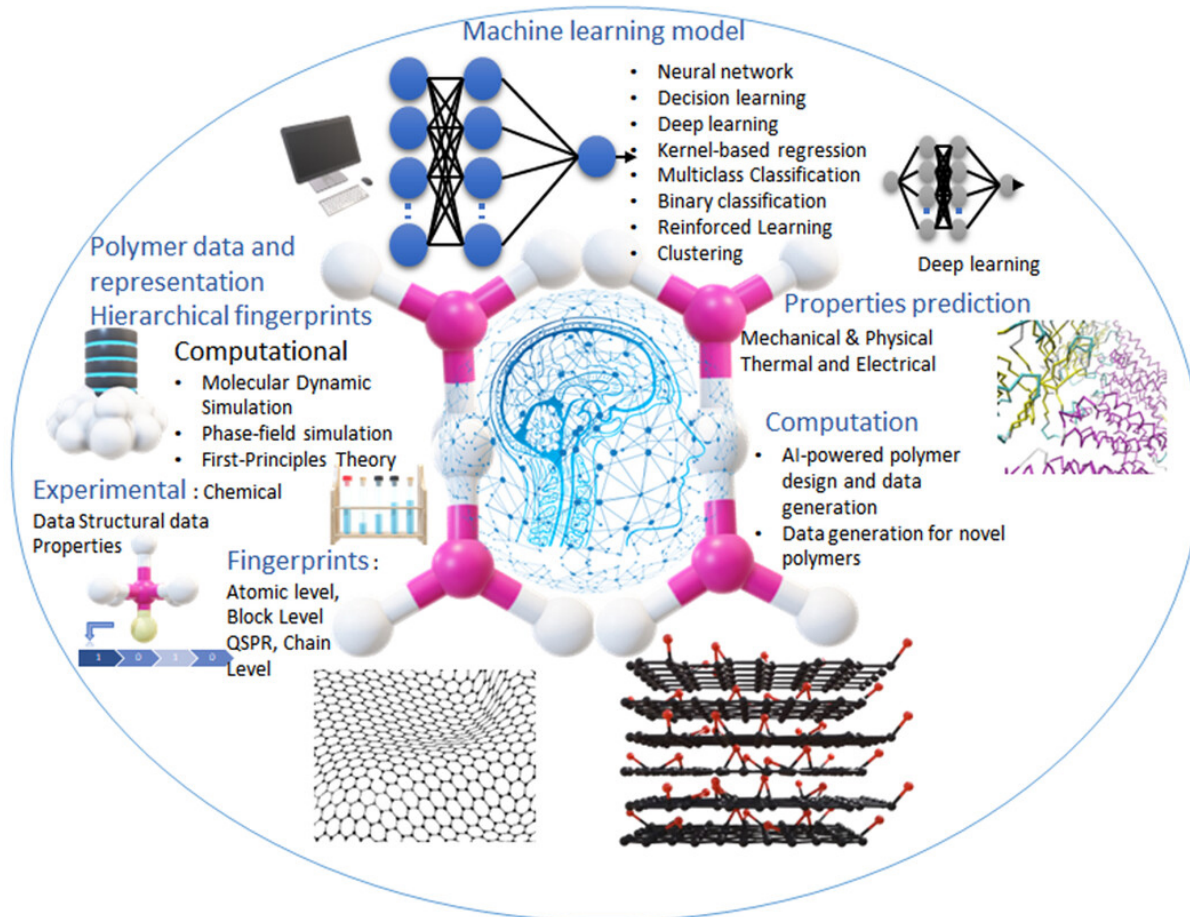


Figure 18. ML technique for developing novel energy storage materials from polymer-nanofiller nanocomposites^[130]. ML: Machine learning.

approximated. For polymer nanocomposites, a detailed calculation (from micrometers to millimeters) is required using a phase field model or a finite element model (FEM)^[131]. Shen *et al.*^[132] utilized ML techniques to evaluate the energy storage capacity of polymer nanocomposites through large-scale phase-field calculations of dielectric reactions, charge transfer, and decomposition mechanisms. Finite element methods and other computational tools are also used to analyze characteristics such as space charge transfer. For example, the bipolar charge transfer framework is used to characterize the space charge distribution in dielectrics related to breakdown robustness^[133].

Nanofiller properties (dielectric constant, conductivity, band gap, thermal conductivity) and interface characteristics (trap states, polarization, core-shell parameters) critically govern nanocomposite behavior, along with geometric factors (shape, volume fraction, distribution, orientation)^[134]. Current characterization methods employ these physical descriptors^[135], enabling process optimization and physics-based understanding. For example, nanofiller morphology, dielectric properties, and concentration directly represent composite performance^[136–137]. As illustrated in Figure 18, ML leverages such descriptors to correlate filler attributes with dielectric behavior and predict energy storage capacity^[138].

Liu *et al.*^[139] adopted a three-variable composite electrothermal breakdown phase field model to simulate the evolution of the breakdown path of polymer composites, analyze the breakdown mechanism, and construct a functional relationship between the E_b and relevant parameters by combining ML to guide the design of high-temperature dielectric polymer-based composites. Liu *et al.*^[140] proposed a conduction model that combines Richardson-Schottky emission with hopping conduction to describe the charge injection and transport in polymer nanocomposites. Through phase-field simulations incorporating electro-thermal-mechanical breakdown mechanisms, they investigated the effects of the volume fraction, size, and permittivity of nanofillers on the dielectric response and breakdown behavior.

ML is a valuable tool for materials science. Consequently, various ML algorithms have been applied to composite modeling and design optimization^[128]. The goal is to design materials with superior, previously unattainable properties.

High entropy strategy

The U_e in a dielectric charge/discharge cycle is defined as

$$U_e = \int_{P_m}^{P_r} E dP \quad (9)$$

In this context, P_m , P_r , and E represent the maximum polarization, residual polarization, and applied electric field, respectively. A significant difference between P_m and P_r , along with a high E_b , results in elevated U_e . Additionally, a high ratio of P_m to P_r , indicating minimal polarization-switching hysteresis, enhances U_e ($\eta = \frac{U_e}{U_e + U_{loss}}$; U_{loss} is the energy loss due to hysteresis). Relaxation ferroelectrics (RFEs) exhibit excellent polarization properties (low P_r , high P_m)^[141], attributed to polar nanoregions from compositional inhomogeneity in multicomponent oxides^[142]. However, the quantitative correlation between nanoscale inhomogeneity and macroscopic relaxor behavior remains unclear, impeding rational design and performance optimization due to a lack of quantitative characterization and control methods.

The local compositional inhomogeneity is closely related to the atomic disorder in the RFE system^[143], so configurational entropy (S_{config}) can be used to assess the local compositional inhomogeneity. S_{config} is defined as $-R[(\sum_{i=1}^N x_i \ln x_i) + (\sum_{j=1}^M x_j \ln x_j)]$, where R , $N(M)$, and x_i (x_j) are the ideal gas constant, atomic species, and content of the equivalent cation (anion) site, respectively^[144]. S_{config} increases as foreign atoms occupy equivalent sites. This results in greater atomic disorder and lattice distortion, attributed to variations in atomic sizes, masses, and electronegativity. Thus, the increase in the S_{config} of the RFE is closely related to the increase in localized compositional inhomogeneities. Recent studies demonstrate entropic strategies can enhance energy storage in linear $Bi_2Ti_2O_7$ via amorphous/crystalline structure control^[145]. Similar approaches using high-entropy components show promise in relaxor ferroelectrics^[146], though entropy's role in relaxor behavior remains unexplored. Conformational entropy, easily calculated from composition, may predict local inhomogeneity and modulate relaxor properties.

The intrinsic dielectric E_b is empirically described as $E_b \propto e^{E_g}$ ^[147]. A wider E_g impedes electron transitions from the valence band to the conduction band. Consequently, this leads to elevated resistivity and enhanced E_b . Moreover, in dielectric materials, the relatively low carrier concentration means that entropy-induced lattice distortions significantly increase electron-lattice atom collisions. This enhanced electron scattering diminishes conductivity and subsequently reinforces the E_b ^[148]. Liu *et al.*^[149] incorporated Ti/Hf into ZrP_2O_7 at ~ 300 °C, inducing lattice distortions that enhanced phonon scattering while suppressing grain growth, ultimately improving thermal stability with $\epsilon_r = 7.59$ -8.47 and $\tan \delta = 8.5 \times 10^{-3}$ - 1.2×10^{-2} at 100-1,100 °C.

Chen *et al.*^[146] developed high-entropy relaxor ferroelectrics with multiphase nanoclusters and oxygen-octahedral tilting, creating ultrasmall polar nanoregions that enhance E_b and delay polarization saturation [Figure 19]. The entropy-stabilized system shows broadened T_c distribution and weakened inter-region coupling, achieving temperature/frequency stability with $U_d = 3.38 \pm 0.20 \text{ J/cm}^3$ ($\eta = 85.8\% \pm 6.0\%$) at 25–140 °C/400 kV/cm. Zhu *et al.*^[150] expanded this strategy in $(\text{Bi}_{0.5}\text{K}_{0.5})\text{TiO}_3$ - based high-entropy RFE ceramics by reducing ion-size mismatch (entropy: 1.54 \rightarrow 2.06 R), attaining $U_d = 18.7 \text{ J/cm}^3$ ($\eta = 85\%$). These approaches enable high-temperature, high-performance dielectric materials for advanced energy storage.

Fan *et al.*^[151] further explored a new design concept and proposed a high-entropy modulation design for the quantum paraelectric-ferroelectric/antiferroelectric matrix. This design enables stable energy charge/discharge across a wide voltage range. In bulk perovskite materials, the recoverable energy density reaches 13.3 J/cm³. Optimized design and processing yield versatile polar, defect-free structures, and the material possesses an E_b of 750 kV/cm.

CONCLUSIONS

Flexible high-temperature dielectric polymer composites (for extreme environments like aerospace) are a current research focus, emphasizing thermal stability, charge storage, and high-temperature discharge behavior. Through optimized material systems, filler/structural design, and innovative methods (e.g., machine learning, high-entropy strategies), their temperature resistance has been significantly improved. Future research will develop novel materials and enhance reliability assessments to facilitate applications [Figure 20].

Dielectric materials store energy in electrostatic form, and their energy storage capacity mainly depends on the dielectric constant and breakdown field strength of the material. At high-temperature circumstances, the molecular motion of materials intensifies, leading to a decrease in dielectric constant and an increase in leakage current, which in turn affects energy storage performance. Through this work, it is known that there are the following methods to improve high-temperature energy storage performance:

- (1) Nanocomposite modification. By introducing inorganic nano fillers (such as Al_2O_3 , boron nitride nanosheets, *etc.*) to enhance the thermal stability and mechanical properties of the polymer matrix, while improving interfacial compatibility to reduce leakage current.
- (2) Design of fully organic nanocomposites. Polymer materials have good structural adjustability and designability, and their thermal stability and durability are improved through physical mixing and molecular structure design of high-temperature polymers.
- (3) Layered structure design. Utilizing the synergistic effect of polymer/ceramic laminated composite materials, the thermal stability of polymer films is enhanced through the nano-confinement effect, thereby achieving high energy storage density at high temperatures.

For future prospects, despite significant progress, polymer-based dielectric materials still face many challenges in the field of high-temperature energy storage, such as multiple interface defects, filler aggregation, and flexibility loss, which weaken the long-term service reliability of the materials.

With the development of nanotechnology and materials science, it is expected that more new flexible dielectric polymer composites with excellent high-temperature energy storage performance will be developed in the future. These materials will play an important role in fields such as new energy vehicles,

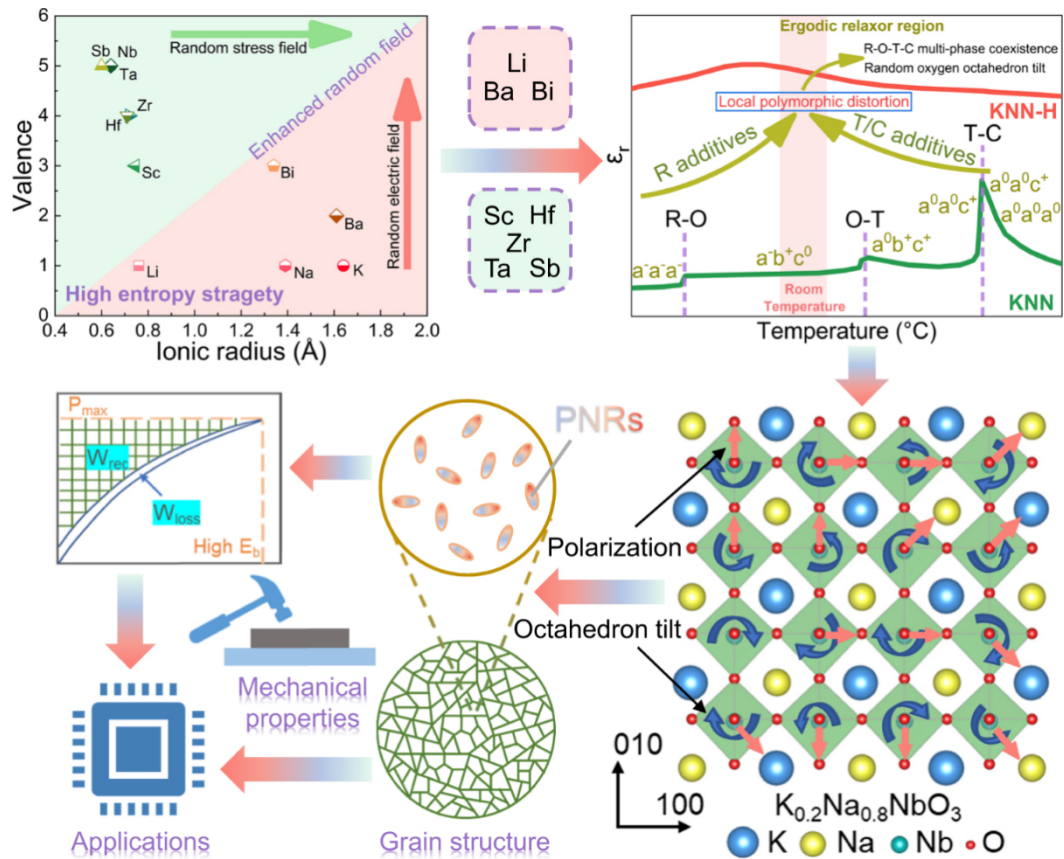


Figure 19. Schematic of high entropy design strategy for localized polymorphic distortion and giant energy storage performance^[146].

aerospace power electronic devices, etc.

(1) Large-scale production and application. Currently, some research results have preliminarily achieved industrial roll-to-roll production, laying the foundation for the large-scale application of flexible dielectric polymer composites. In the future, it is necessary to further optimize production processes, reduce costs, and improve product consistency and reliability.

(2) Multifunctionality and Integration. With the development of electronic devices toward miniaturization and multifunctionality, flexible dielectric polymer composites will not only be limited to energy storage functions in the future, but may also integrate multiple functions such as sensing and driving, forming more intelligent and efficient systems.

(3) Environmentally friendly and sustainable development. While pursuing high performance, future research will also pay more attention to the environmental friendliness and sustainability of materials. Developing biodegradable and recyclable flexible dielectric polymer composites will become an important direction.

In summary, significant progress has been made in the study of energy storage and mechanisms of flexible dielectric polymer composites in high-temperature environments, but many challenges still remain. In the future, it is necessary to continue to strengthen basic research and application development work, and

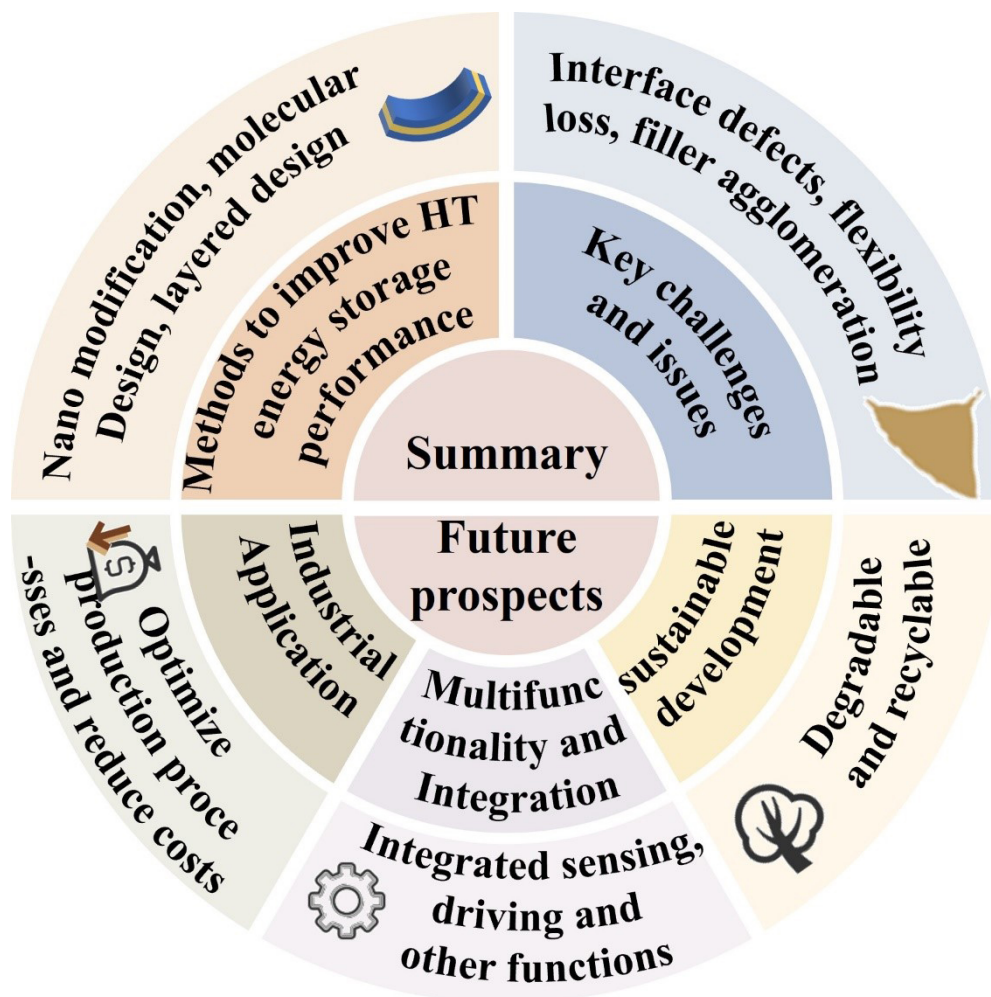


Figure 20. The summary and future prospects of flexible, high-temperature-resistant composite dielectric energy storage materials.

promote the continuous development of this field.

DECLARATIONS

Authors' contributions

Writing original draft: Zhao, L.

Review & editing, supervision: Zhang, F.; Hu, H.

Availability of data and materials

Not applicable.

Financial support and sponsorship

The research was supported by the National Natural Science Foundation of China (52402164).

Conflicts of interest

Hu H is the Guest Editor of the Special Issue “*Unraveling the Dynamic Interplay between Microstructure and Functional Characteristics in Advanced Electroceramics*”. He is not involved in any steps of editorial processing, notably including reviewer selection, manuscript handling, and decision making. The other

authors declared that there are no conflicts of interest.

Ethical approval and consent to participate

Not applicable.

Consent for publication

Not applicable.

Copyright

© The Author(s) 2025.

REFERENCES

- Chen, J.; Zhou, Y.; Huang, X.; et al. Ladderphane copolymers for high-temperature capacitive energy storage. *Nature* **2023**, *615*, 62–6. DOI
- Kim, J.; Saremi, S.; Acharya, M.; et al. Ultrahigh capacitive energy density in ion-bombarded relaxor ferroelectric films. *Science* **2020**, *369*, 81–4. DOI
- Yang, B.; Zhang, Q.; Huang, H.; et al. Engineering relaxors by entropy for high energy storage performance. *Nat. Energy*. **2023**, *8*, 956–64. DOI
- Johnson, R.; Evans, J.; Jacobsen, P.; Thompson, J.; Christopher, M. The changing automotive environment: high-temperature electronics. *IEEE. Trans. Electron. Packag. Manufact.* **2004**, *27*, 164–76. DOI
- Weimer, J. A.; Electrical, In *AIAA/IEEE Digital Avionics Systems Conference, Proceedings of AIAA/IEEE Digital Avionics Systems Conference*, Fort Worth, TX, USA, October 25–28; IEEE Publishers: Piscataway, New Jersey, USA, 1993; pp 445–450. DOI
- Wu, C.; Deshmukh, A. A.; Li, Z.; et al. Flexible temperature-invariant polymer dielectrics with large bandgap. *Adv Mater* **2020**;32:e2000499.[DOI:10.1002/adma.202000499] Caution!
- Global Power Capacitor Markets in 2020: Expect Slow and Steady Market Growth. Available from: <https://www.tti.com/content/ttiinc/en/resources/marketeye/categories/passives/me-zogbi-20200309.html> [accessed on 29 May 2025].
- Li, Q.; Chen, L.; Gadinski, M. R.; et al. Flexible high-temperature dielectric materials from polymer nanocomposites. *Nature* **2015**, *523*, 576–9. DOI
- Li, H.; Zhou, Y.; Liu, Y.; Li, L.; Liu, Y.; Wang, Q. Dielectric polymers for high-temperature capacitive energy storage. *Chem. Soc. Rev.* **2021**, *50*, 6369–400. DOI
- Li, S.; Dong, J.; Niu, Y.; et al. Enhanced high-temperature energy storage properties of polymer composites by interlayered metal nanodots. *J. Mater. Chem. A*. **2022**, *10*, 18773–81. DOI
- Yuan, C.; Zhou, Y.; Zhu, Y.; et al. Polymer/molecular semiconductor all-organic composites for high-temperature dielectric energy storage. *Nat. Commun.* **2020**, *11*, 3919. DOI PubMed PMC
- Wei, R.; Zhan, C.; Yang, Y.; He, P.; Liu, X. Polyarylene ether nitrile and titanium dioxide hybrids as thermal resistant dielectrics. *Chin. J. Polym. Sci.* **2021**, *39*, 211–8. DOI
- You, Y.; Liu, S.; Tu, L.; et al. Controllable fabrication of poly(arylene ether nitrile) dielectrics for thermal-resistant film capacitors. *Macromolecules* **2019**, *52*, 5850–9. DOI
- Zhang, T.; Chen, X.; Thakur, Y.; et al. A highly scalable dielectric metamaterial with superior capacitor performance over a broad temperature. *Sci. Adv.* **2020**, *6*, eaax6622. DOI PubMed PMC
- Huan, T. D.; Boggs, S.; Teyssedre, G.; et al. Advanced polymeric dielectrics for high energy density applications. *Prog. Mater. Sci.* **2016**, *83*, 236–69. DOI
- Kim, M. P.; Um, D. S.; Shin, Y. E.; Ko, H. High-performance triboelectric devices via dielectric polarization: a review. *Nanoscale. Res. Lett.* **2021**, *16*, 35. DOI PubMed PMC
- Nan, C.; Shen, Y.; Ma, J. Physical properties of composites near percolation. *Annu. Rev. Mater. Res.* **2010**, *40*, 131–51. DOI
- Fan, B.; Zhou, M.; Zhang, C.; He, D.; Bai, J. Polymer-based materials for achieving high energy density film capacitors. *Prog. Polym. Sci.* **2019**, *97*, 101143. DOI
- Dong, J.; Deng, X.; Niu, Y.; Pan, Z.; Wang, H. Research progress of polymer based dielectrics for high-temperature capacitor energy storage. *Acta. Phys. Sin.* **2020**, *69*, 217701. DOI
- Qiu, J.; Gu, Q.; Sha, Y.; Huang, Y.; Zhang, M.; Luo, Z. Preparation and application of dielectric polymers with high permittivity and low energy loss: a mini review. *J. Appl. Polym. Sci.* **2022**, *139*, 52367. DOI
- O'Hara, A.; Balke, N.; Pantelides, S. T. Unique features of polarization in ferroelectric ionic conductors. *Adv. Elect. Mater.* **2022**, *8*, 2100810. DOI
- Dakin, T. Conduction and polarization mechanisms and trends in dielectric. *IEEE. Electr. Insul. Mag.* **2006**, *22*, 11–28. DOI
- Huang, S.; Liu, K.; Zhang, W.; et al. All-organic polymer dielectric materials for advanced dielectric capacitors: theory, property, modified design and future prospects. *Polym. Rev.* **2023**, *63*, 515–73. DOI

24. Thakur VK, Gupta RK. Recent progress on ferroelectric polymer-based nanocomposites for high energy density capacitors: synthesis, dielectric properties, and future aspects. *Chem. Rev.* **2016**, *116*, 4260-317. DOI PubMed
25. Baldwin, A. F.; Ma, R.; Huan, T. D.; Cao, Y.; Ramprasad, R.; Sotzing, G. A. Effect of incorporating aromatic and chiral groups on the dielectric properties of poly(dimethyltin esters). *Macromol. Rapid. Commun.* **2014**, *35*, 2082-8. DOI
26. Chen, Y.; Du, Y. K.; Yue, Y. C.; et al. Correlation between energy storage density and differential dielectric constant in ferroelectrics. *J. Elec. Materi.* **2020**, *49*, 659-67. DOI
27. Wei, J.; Zhu, L. Intrinsic polymer dielectrics for high energy density and low loss electric energy storage. *Prog. Polym. Sci.* **2020**, *106*, 101254. DOI
28. Chen, J.; Pei, Z.; Chai, B.; et al. Engineering the dielectric constants of polymers: from molecular to mesoscopic scales. *Adv. Mater.* **2024**, *36*, e2308670. DOI
29. Kao, K. C.; Dielectric, P. S.; 1st,; San Diego: Academic Press. 2004, p573.
30. Mannodi-kanakkithodi, A.; Huan, T. D.; Ramprasad, R. Mining materials design rules from data: the example of polymer dielectrics. *Chem. Mater.* **2017**, *29*, 9001-10. DOI
31. Rui, G.; Allahyarov, E.; Thomas, J. J.; Taylor, P. L.; Zhu, L. Temperature-dependent rotational dipole mobility and devitrification of the rigid amorphous fraction in unpoled and poled biaxially oriented poly(vinylidene fluoride). *Macromolecules* **2022**, *55*, 9705-14. DOI
32. Zhu, Y.; Zhang, Z.; Litt, M. H.; Zhu, L. High dielectric constant sulfonyl-containing dipolar glass polymers with enhanced orientational polarization. *Macromolecules* **2018**, *51*, 6257-66. DOI
33. Zapsas, G.; Patil, Y.; Gnanou, Y.; Ameduri, B.; Hadjichristidis, N. Poly(vinylidene fluoride)-based complex macromolecular architectures: from synthesis to properties and applications. *Prog. Polym. Sci.* **2020**, *104*, 101231. DOI
34. Rui, G.; Huang, Y.; Chen, X.; et al. Giant spontaneous polarization for enhanced ferroelectric properties of biaxially oriented poly(vinylidene fluoride) by mobile oriented amorphous fractions. *J. Mater. Chem. C.* **2021**, *9*, 894-907. DOI
35. Zhang, G.; Li, Y.; Tang, S.; Thompson, R. D.; Zhu, L. The role of field electron emission in polypropylene/aluminum nanodielectrics under high electric fields. *ACS. Appl. Mater. Interfaces.* **2017**, *9*, 10106-19. DOI
36. Hardy, C. G.; Islam, M. S.; Gonzalez-delozier, D.; et al. Converting an electrical insulator into a dielectric capacitor: end-capping polystyrene with oligoaniline. *Chem. Mater.* **2013**, *25*, 799-807. DOI
37. Yang, M.; Guo, M.; Xu, E.; et al. Polymer nanocomposite dielectrics for capacitive energy storage. *Nat. Nanotechnol.* **2024**, *19*, 588-603. DOI
38. Collins, J.; Gourdin, G.; Foster, M.; Qu, D. Carbon surface functionalities and SEI formation during Li intercalation. *Carbon* **2015**, *92*, 193-244. DOI
39. Jian, G.; Jiao, Y.; Feng, L.; et al. High energy density of BaTiO₃@TiO₂ nanosheet/polymer composites via ping-pong-like electron area scattering and interface engineering. *NPG. Asia. Mater.* **2022**, *14*, 356. DOI
40. Luo, D.; Wang, W.; Feng, W.; Liu, S.; He, B.; Liu, Y. Achieving high energy density and efficiency concurrently in BNNS/P(VDF-HFP) composites via synchronous heating and stirring treatment. *J. Energy. Storage.* **2024**, *82*, 110553. DOI
41. Zhu, T.; Zhao, H.; Zhang, N.; Zhang, C.; Bai, J. Tuning the MOF-derived Fe fillers and crystal structure of PVDF composites for enhancement of their energy storage density. *Chem. Eng. J.* **2024**, *482*, 149204. DOI
42. Mukherjee, A.; Dasgupta, G. B.; Roy, S.; Lim, G. K. Ultra strong flexible Ba_{0.7}Sr_{0.3}Zr_{0.02}Ti_{0.98}O₃/MWCNT/PVDF Nanocomposites: Pioneering material with remarkable energy storage for self-powered devices. *Chem. Eng. J.* **2024**, *488*, 151014. DOI
43. Liu, Y.; Tang, B.; Wang, Z.; et al. Enhanced dielectric performances of strontium barium titanate nanorod composites via improved interfacial compatibility. *J. Colloid. Interface. Sci.* **2025**, *680*, 85-95. DOI
44. Chen, J.; Zhang, X.; Wang, Z.; Chen, W.; Yuan, Q.; Wang, Y. Laminated ferroelectric polymer composites exhibit synchronous ultrahigh discharge efficiency and energy density via utilizing multiple-interface barriers. *J. Mater. Chem. A.* **2022**, *10*, 20402-13. DOI
45. Guo, R.; Luo, H.; Zhai, D.; et al. Bilayer structured PVDF-based composites via integrating BaTiO₃ nanowire arrays and BN nanosheets for high energy density capacitors. *Chem. Eng. J.* **2022**, *437*, 135497. DOI
46. Sun, L.; Shi, Z.; Liang, L.; et al. Concurrently achieving high discharged energy density and efficiency in composites by introducing ultralow loadings of core-shell structured graphene@TiO₂ nanoboxes. *ACS. Appl. Mater. Interfaces.* **2022**, *14*, 29292-301. DOI
47. Zheng, Y.; Dai, Z.; Liu, C.; et al. High energy storage properties for dielectric composite by asymmetric three-layer films design. *J. Energy. Storage.* **2024**, *93*, 112387. DOI
48. Li, W.; Liang, R.; Yang, L.; et al. Novel plum pudding structured BaTiO₃@ZIF-67 filler design for high-performance dielectric polymer composites. *J. Energy. Storage.* **2024**, *91*, 112010. DOI
49. Gao, L.; Zhang, J.; Song, L.; Bai, X.; Yu, C. Low-content core-shell-structured TiO₂ nanobelts@SiO₂ doped with poly(vinylidene fluoride) composites to achieve high-energy storage density. *J. Mater. Sci.: Mater. Electron.* **2022**, *33*, 18345-55. DOI
50. Chen, J.; Huang, F.; Zhang, C.; Meng, F.; Cao, L.; Lin, H. Enhanced energy storage density in poly(vinylidene fluoride-hexafluoropropylene) nanocomposites by filling with core-shell structured BaTiO₃@MgO nanoparticles. *J. Energy. Storage.* **2022**, *53*, 105163. DOI
51. Zhao, D.; Cai, Q.; Zhu, X.; et al. Multilayer dielectric nanocomposites with cross-linked dielectric transition interlayers for high-temperature applications. *ACS. Appl. Mater. Interfaces.* **2022**, *14*, 42531-40. DOI

52. Yu, X.; Yang, R.; Zhang, W.; et al. Interface engineering of polymer composite films for high-temperature capacitive energy storage. *Chem. Eng. J.* **2024**, *496*, 154056. DOI
53. Xie, H.; Luo, H.; Pei, Z.; Chen, S.; Zhang, D. Improved discharge energy density and efficiency of polypropylene-based dielectric nanocomposites utilizing BaTiO₃@TiO₂ nanoparticles. *Mater. Today. Energy.* **2022**, *30*, 101160. DOI
54. Zhang, F.; Wang, G.; Lin, N.; et al. Synergistic promotion of inter-particle and intra-particle polarizations in BST@TiO₂/PVDF nanocomposites towards elevated dielectric properties. *Compos. Sci. Technol.* **2024**, *251*, 110547. DOI
55. Ding, C.; Tang, X.; Yu, S.; et al. Concurrently enhanced dielectric properties and energy density in poly(vinylidene fluoride)-based core-shell BaTiO₃ nanocomposites via constructing a polar and rigid polymer interfacial layer. *J. Mater. Chem. C.* **2022**, *10*, 6323-33. DOI
56. Wang, P.; Guo, Z.; Sun, Z.; Li, G.; Bi, J.; Qian, L. Carrier gradient core-double shell structure with heterojunction transition layer for significantly enhancing dielectric properties. *Chem. Eng. J.* **2024**, *496*, 153968. DOI
57. Jing, L.; Li, W.; Gao, C.; Li, M.; Fei, W. Achieving high energy storage performance in BiFeO₃@TiO₂ filled PVDF-based composites with opposite double heterojunction via electric field tailoring. *Chem. Eng. J.* **2022**, *450*, 138143. DOI
58. Xu, H.; Xie, C.; Gou, B.; Wang, R.; Zhou, J.; Li, L. Core-double-shell structured BT@TiO₂@PDA and oriented BNNs doped epoxy nanocomposites with field-dependent nonlinear electrical properties and enhancing breakdown strength. *Compos. Sci. Technol.* **2022**, *230*, 109777. DOI
59. Li, X.; Wang, Y.; Rao, Y.; Ma, X.; Yang, Y.; Zhang, J. Enhanced energy storage in PVDF-based nanocomposite capacitors through (001)-oriented BaTiO₃ single-crystal platelets. *ACS. Appl. Mater. Interfaces.* **2024**, *16*, 27785-93. DOI
60. Wang, T.; Deng, Y.; Sun, H.; Wang, D.; Zhang, M. Enhancing energy storage performance of PVDF-based composites through semiconducting AZO-BT heterostructure. *J. Energy. Storage.* **2024**, *82*, 110541. DOI
61. Wang, F.; Luo, H.; Zhai, D.; et al. Dielectric nanocomposites with high energy density by doping core-double shell structured fillers. *Compos. Part. A: Appl. Sci. Manuf.* **2022**, *159*, 107019. DOI
62. Zhang, Z.; Zhou, L.; Wang, L.; Hao, Q.; Hua, X.; Wei, R. Enhancing energy storage density of poly(arylene ether nitrile) via incorporating modified barium titanate nanorods and hot-stretching. *Nano. Res.* **2024**, *17*, 7574-84. DOI
63. Sun, X.; Zheng, Y.; Liu, K.; et al. Gradient core-shell structure enabling high energy storage performances in PVDF-based copolymers. *J. Mater. Chem. A.* **2024**, *12*, 8216-25. DOI
64. Chen, C.; Wang, S.; Gong, Z.; et al. Stable dielectric properties at high-temperature of Al₂O₃-PESU composite for energy storage application. *Compos. Part. A: Appl. Sci. Manuf.* **2024**, *181*, 108109. DOI
65. Meng, G.; She, J.; Wang, C.; Wang, W.; Pan, C.; Cheng, Y. Sandwich-structured h-BN/PVDF/h-BN film with high dielectric strength and energy storage density. *Front. Chem.* **2022**, *10*, 910305. DOI PubMed PMC
66. Shang, Y.; Feng, Y.; Meng, Z.; Zhang, C.; Zhang, T.; Chi, Q. Achieving synergistic improvement in dielectric and energy storage properties at high-temperature of all-organic composites via physical electrostatic effect. *Mater. Horiz.* **2024**, *11*, 1528-38. DOI
67. Yang, T.; Wang, C.; Liu, L.; Zhang, L. Silicone elastomer dielectric composites by introducing novel O-MMT@TiO₂ nanoparticles for energy harvesting application. *Composites. Part. A: Appl. Sci. Manuf.* **2024**, *185*, 108351. DOI
68. Ma, J.; Zhang, Y.; Miao, L.; Zhang, L.; Zhang, S.; Jiang, X. Combining covalent bonding interface among different components and controlled orientation of one-dimensional nanofibers for high energy density nanocomposites. *Compos. Part. B: Eng.* **2022**, *243*, 110134. DOI
69. Zuo, B.; Zhou, H.; Davis, M. J. B.; Wang, X.; Priestley, R. D. Effect of local chain conformation in adsorbed nanolayers on confined polymer molecular mobility. *Phys. Rev. Lett.* **2019**, *122*, 217801. DOI PubMed
70. Papon, A.; Montes, H.; Hanafi, M.; Lequeux, F.; Guy, L.; Saalwächter, K. Glass-transition temperature gradient in nanocomposites: evidence from nuclear magnetic resonance and differential scanning calorimetry. *Phys. Rev. Lett.* **2012**, *108*, 065702. DOI PubMed
71. Ediger, M. D.; Forrest, J. A. Dynamics near free surfaces and the glass transition in thin polymer films: a view to the future. *Macromolecules* **2014**, *47*, 471-8. DOI
72. Rittigstein, P.; Priestley, R. D.; Broadbelt, L. J.; Torkelson, J. M. Model polymer nanocomposites provide an understanding of confinement effects in real nanocomposites. *Nat. Mater.* **2007**, *6*, 278-82. DOI PubMed
73. Wan, B.; Dong, X.; Yang, X.; et al. Rising of dynamic polyimide materials: a versatile dielectric for electrical and electronic applications. *Adv. Mater.* **2023**, *35*, e2301185. DOI
74. Ho, J. S.; Greenbaum, S. G. Polymer capacitor dielectrics for high temperature applications. *ACS. Appl. Mater. Interfaces.* **2018**, *10*, 29189-218. DOI PubMed
75. Qiao, Y.; Yin, X.; Zhu, T.; Li, H.; Tang, C. Dielectric polymers with novel chemistry, compositions and architectures. *Prog. Polym. Sci.* **2018**, *80*, 153-62. DOI
76. Deshmukh, A. A.; Wu, C.; Yassin, O.; et al. Flexible polyolefin dielectric by strategic design of organic modules for harsh condition electrification. *Energy. Environ. Sci.* **2022**, *15*, 1307-14. DOI
77. Wang, R.; Zhu, Y.; Fu, J.; et al. Designing tailored combinations of structural units in polymer dielectrics for high-temperature capacitive energy storage. *Nat. Commun.* **2023**, *14*, 2406. DOI PubMed PMC
78. Zhu, T.; Zhao, H.; Zhang, N.; et al. Ultrahigh energy storage density in poly(vinylidene fluoride)-based composite dielectrics via constructing the electric potential well. *Adv. Energy. Mater.* **2023**, *13*, 2203587. DOI
79. Yu, S.; Liu, Y.; Ding, C.; et al. All-organic sandwich structured polymer dielectrics with polyimide and PVDF for high temperature capacitor application. *J. Energy. Storage.* **2023**, *62*, 106868. DOI

80. Bao, Z.; Du, X.; Ding, S.; et al. Improved working temperature and capacitive energy density of biaxially oriented polypropylene films with alumina coating layers. *ACS Appl. Energy Mater.* **2022**, *5*, 3119-28. DOI
81. Ping, J. B.; Feng, Q. K.; Zhang, Y. X.; et al. A bilayer high-temperature dielectric film with superior breakdown strength and energy storage density. *Nanomicro. Lett.* **2023**, *15*, 154. DOI PubMed PMC
82. Zha, J.; Xiao, M.; Wan, B.; Wang, X.; Dang, Z.; Chen, G. Polymer dielectrics for high-temperature energy storage: Constructing carrier traps. *Prog. Mater. Sci.* **2023**, *140*, 101208. DOI
83. Li, X.; Liu, B.; Wang, J.; et al. High-temperature capacitive energy storage in polymer nanocomposites through nanoconfinement. *Nat. Commun.* **2024**, *15*, 6655. DOI PubMed PMC
84. Guo, M.; Jiang, J.; Shen, Z.; Lin, Y.; Nan, C.; Shen, Y. High-energy-density ferroelectric polymer nanocomposites for capacitive energy storage: enhanced breakdown strength and improved discharge efficiency. *Mater. Today.* **2019**, *29*, 49-67. DOI
85. Li, X.; He, S.; Jiang, Y.; et al. Unraveling bilayer interfacial features and their effects in polar polymer nanocomposites. *Nat. Commun.* **2023**, *14*, 5707. DOI PubMed PMC
86. Zhou, Y.; Wang, Q. Advanced polymer dielectrics for high temperature capacitive energy storage. *J. Appl. Phys.* **2020**, *127*, 240902. DOI
87. Vanherck, K.; Koeckelberghs, G.; Vankelecom, I. F. Crosslinking polyimides for membrane applications: a review. *Prog. Polym. Sci.* **2013**, *38*, 874-96. DOI
88. Zhou, Y.; Li, Q.; Dang, B.; et al. A Scalable, high-throughput, and environmentally benign approach to polymer dielectrics exhibiting significantly improved capacitive performance at high temperatures. *Adv. Mater.* **2018**, *30*, e1805672. DOI
89. Venkat, N.; Dang, T. D.; Bai, Z.; et al. High temperature polymer film dielectrics for aerospace power conditioning capacitor applications. *Mater. Sci. Eng.: B.* **2010**, *168*, 16-21. DOI
90. Feng, Y.; Zhou, Y.; Zhang, T.; et al. Ultrahigh discharge efficiency and excellent energy density in oriented core-shell nanofiber-polyetherimide composites. *Energy. Storage. Mater.* **2020**, *25*, 180-92. DOI
91. Zou, K.; Dan, Y.; Yu, Y.; et al. Flexible dielectric nanocomposites with simultaneously large discharge energy density and high energy efficiency utilizing (Pb,Lu)(Zr,Sn,Ti)O₃ antiferroelectric nanoparticles as fillers. *J. Mater. Chem. A.* **2019**, *7*, 13473-82. DOI
92. Wang, S.; Huang, X.; Wang, G.; Wang, Y.; He, J.; Jiang, P. Increasing the energy efficiency and breakdown strength of high-energy-density polymer nanocomposites by engineering the Ba_{0.7}Sr_{0.3}TiO₃ nanowire surface via reversible addition-fragmentation chain transfer polymerization. *J. Phys. Chem. C.* **2015**, *119*, 25307-18. DOI
93. Huang, X.; Jiang, P. Core-shell structured high-k polymer nanocomposites for energy storage and dielectric applications. *Adv. Mater.* **2015**, *27*, 546-54. DOI PubMed
94. Yu, K.; Wang, H.; Zhou, Y.; Bai, Y.; Niu, Y. Enhanced dielectric properties of BaTiO₃/poly(vinylidene fluoride) nanocomposites for energy storage applications. *J. Appl. Phys.* **2013**, *113*, 034105. DOI
95. Hu, P.; Sun, W.; Fan, M.; et al. Large energy density at high-temperature and excellent thermal stability in polyimide nanocomposite contained with small loading of BaTiO₃ nanofibers. *Appl. Surf. Sci.* **2018**, *458*, 743-50. DOI
96. Sun, W.; Lu, X.; Jiang, J.; et al. Dielectric and energy storage performances of polyimide/BaTiO₃ nanocomposites at elevated temperatures. *J. Appl. Phys.* **2017**, *121*, 244101. DOI
97. Shen, Z.; Wang, J.; Jiang, J.; et al. Phase-field model of electrothermal breakdown in flexible high-temperature nanocomposites under extreme conditions. *Adv. Energy Mater.* **2018**, *8*, 1800509. DOI
98. Wang, P.; Guo, Y.; Zhou, D.; et al. High-temperature flexible nanocomposites with ultra-high energy storage density by nanostructured MgO fillers. *Adv. Funct. Mater.* **2022**, *32*, 2204155. DOI
99. Zhu, Y.; Zhu, Y.; Huang, X.; et al. High energy density polymer dielectrics interlayered by assembled boron nitride nanosheets. *Adv. Energy Mater.* **2019**, *9*, 1903062. DOI
100. Li, H.; Ai, D.; Ren, L.; et al. Scalable polymer nanocomposites with record high-temperature capacitive performance enabled by rationally designed nanostructured inorganic fillers. *Adv. Mater.* **2019**, *31*, e1900875. DOI
101. Ai, D.; Li, H.; Zhou, Y.; et al. Tuning nanofillers in *in situ* prepared polyimide nanocomposites for high-temperature capacitive energy storage. *Adv. Energy Mater.* **2020**, *10*, 1903881. DOI
102. Liu, F.; Li, Q.; Li, Z.; et al. Poly(methyl methacrylate)/boron nitride nanocomposites with enhanced energy density as high temperature dielectrics. *Composites. Science. and. Technology.* **2017**, *142*, 139-44. DOI
103. Li, X.; Luo, H.; Zhai, D.; et al. Enhanced capacitive energy storage of polyetherimide at high temperatures by integration of electrical insulation and thermal conductivity. *Adv. Powder. Mater.* **2025**, *4*, 100286. DOI
104. Thakur, Y.; Zhang, T.; Iacob, C.; et al. Enhancement of the dielectric response in polymer nanocomposites with low dielectric constant fillers. *Nanoscale* **2017**, *9*, 10992-7. DOI
105. Yang, M.; Li, H.; Wang, J.; et al. Roll-to-roll fabricated polymer composites filled with subnanosheets exhibiting high energy density and cyclic stability at 200 °C. *Nat. Energy.* **2024**, *9*, 143-53. DOI
106. Chadband, W. G. Electrical degradation and breakdown in polymers. *IEEE. Rev.* **1992**, *38*, 404. DOI
107. Thakur, Y.; Lean, M. H.; Zhang, Q. M. Reducing conduction losses in high energy density polymer using nanocomposites. *Appl. Phys. Lett.* **2017**, *110*, 122905. DOI
108. Liu, J.; Shen, Z.; Xu, W.; et al. Interface-strengthened polymer nanocomposites with reduced dielectric relaxation exhibit high energy density at elevated temperatures utilizing a facile dual crosslinked network. *Small* **2020**, *16*, e2000714. DOI
109. Xu, W.; Liu, J.; Chen, T.; et al. Bioinspired polymer nanocomposites exhibit giant energy density and high efficiency at high

- temperature. *Small* **2019**, *15*, e1901582. DOI
110. Wang, Z.; Zhao, Y.; Yang, M.; et al. Surface strengthening of polymer composite dielectrics for superior high-temperature capacitive energy storage. *Adv. Energy. Mater.* **2025**, *15*, 2405411. DOI
 111. Bonardd, S.; Moreno-Serna, V.; Kortaberria, G.; Díaz, D. D.; Leiva, A.; Saldías, C. Dipolar glass polymers containing polarizable groups as dielectric materials for energy storage applications. A minireview. *Polymers. (Basel)*. **2019**, *11*, 317. DOI PubMed PMC
 112. Zhuang, Y.; Seong, J. G.; Lee, Y. M. Polyimides containing aliphatic/alicyclic segments in the main chains. *Prog. Polym. Sci.* **2019**, *92*, 35-88. DOI
 113. Ding, S.; Bao, Z.; Wang, Y.; et al. Excellent high-temperature dielectric energy storage of flexible all-organic polyetherimide/poly(arylene ether urea) polymer blend films. *J. Power. Sources.* **2023**, *570*, 233053. DOI
 114. Zhang, Q.; Chen, X.; Zhang, B.; et al. High-temperature polymers with record-high breakdown strength enabled by rationally designed chain-packing behavior in blends. *Matter* **2021**, *4*, 2448-59. DOI
 115. Feng, Q.; Liu, D.; Zhang, Y.; et al. Significantly improved high-temperature charge-discharge efficiency of all-organic polyimide composites by suppressing space charges. *Nano. Energy.* **2022**, *99*, 107410. DOI
 116. Zhang, T.; Shi, B.; Zhang, S.; et al. Nanoscale phase separation achieved through trace PVDF/PEI blending enhances mechanical and energy storage performance at high temperatures. *J. Power. Sources.* **2024**, *620*, 235255. DOI
 117. Xing, K.; Hao, Y.; Wang, X. J.; et al. Enhanced energy storage performance of nano-submicron structural dielectric films by suppressed ferroelectric phase aggregation. *Nat. Commun.* **2025**, *16*, 2006. DOI PubMed PMC
 118. Yang, M.; Yuan, F.; Shi, W.; et al. Sub-nanowires boost superior capacitive energy storage performance of polymer composites at high temperatures. *Adv. Funct. Mater.* **2023**, *33*, 2214100. DOI
 119. Yang, M.; Ren, W.; Jin, Z.; Xu, E.; Shen, Y. Enhanced high-temperature energy storage performances in polymer dielectrics by synergistically optimizing band-gap and polarization of dipolar glass. *Nat. Commun.* **2024**, *15*, 8647. DOI PubMed PMC
 120. Sun, S.; Shi, Z.; Sun, L.; et al. Achieving concurrent high energy density and efficiency in all-polymer layered paraelectric/ferroelectric composites via introducing a moderate layer. *ACS. Appl. Mater. Interfaces.* **2021**, *13*, 27522-32. DOI
 121. Wang, J.; Xie, Y.; Zhang, Y.; et al. The ultrahigh discharge efficiency and energy density of P(VDF-HFP) via electrospinning-hot press with St-MMA copolymer. *Mater. Chem. Front.* **2021**, *5*, 3646-56. DOI
 122. Liu, X. J.; Zhong, S. L.; Zheng, M. S.; Dang, Z. M.; Chen, G.; Zha, J. W. Enhanced high-temperature capacitive performance of a bilayer-structured composite film employing a charge blocking layer. *ACS. Appl. Mater. Interfaces.* **2023**, *15*, 1105-14. DOI PubMed
 123. Guo, Y.; Zhao, W.; Li, D.; et al. Ultra-high capacitive energy storage density at 150 °C achieved in polyetherimide composite films by filler and structure design. *Adv. Mater.* **2025**, *37*, e2415652. DOI
 124. Zhang, D.; Li, Y.; Li, Y.; et al. Synergistically enhanced dielectric, insulating and thermally conductive performances of sandwich PMMA based dielectric films. *Prog. Nat. Sci.: Mater. Int.* **2024**, *34*, 591-7. DOI
 125. Zhou, C.; Xu, W.; Zhang, Y.; et al. Hydrogen bonding of aramid boosts high-temperature capacitive properties of polyetherimide blends. *ACS. Appl. Mater. Interfaces.* **2023**, *15*, 8471-9. DOI
 126. Niu, Y.; Dong, J.; He, Y.; et al. Significantly enhancing the discharge efficiency of sandwich-structured polymer dielectrics at elevated temperature by building carrier blocking interface. *Nano. Energy.* **2022**, *97*, 107215. DOI
 127. Sun, L.; Zhang, F.; Li, L.; et al. Superior capacitive energy storage enabled by molecularly interpenetrating interfaces in layered polymers. *Adv. Mater.* **2025**, *37*, e2412561. DOI
 128. Chen, C. P.; Cheng, C. Y.; Zou, H.; et al. Evaluation of cost-effectiveness of peginterferon plus ribavirin for chronic hepatitis C treatment and direct-acting antiviral agents among HIV-infected patients in the prison and community settings. *J. Microbiol. Immunol. Infect.* **2019**, *52*, 556-62. DOI
 129. Shen, Z.; Liu, H.; Shen, Y.; Hu, J.; Chen, L.; Nan, C. Machine learning in energy storage materials. *InterdiscMat* **2022**, *1*, 175-95. DOI
 130. Bera, S.; Singh, M.; Thantirige, R.; et al. 2D-nanofiller-based polymer nanocomposites for capacitive energy storage applications. *Small. Sci.* **2023**, *3*, 2300016. DOI PubMed PMC
 131. Zhang, T.; Wu, X.; Luo, T. Polymer nanofibers with outstanding thermal conductivity and thermal stability: fundamental linkage between molecular characteristics and macroscopic thermal properties. *J. Phys. Chem. C.* **2014**, *118*, 21148-59. DOI
 132. Shen, Z. H.; Wang, J. J.; Lin, Y.; Nan, C. W.; Chen, L. Q.; Shen, Y. High-throughput phase-field design of high-energy-density polymer nanocomposites. *Adv. Mater.* **2018**, *30*, 1704380. DOI
 133. Wang, C.; Pilania, G.; Boggs, S.; Kumar, S.; Breneman, C.; Ramprasad, R. Computational strategies for polymer dielectrics design. *Polymer* **2014**, *55*, 979-88. DOI
 134. Roy, S. L.; Teyssedre, G.; Laurent, C.; Montanari, G. C.; Palmieri, F. Description of charge transport in polyethylene using a fluid model with a constant mobility: fitting model and experiments. *J. Phys. D.: Appl. Phys.* **2006**, *39*, 1427-36. DOI
 135. Chen, J.; Gao, Y.; Zhu, M.; Li, J.; Yu, Q. Space charge dynamics in double-layered insulation cable under polarity reversal voltage. *IEEE. Trans. Dielect. Electr. Insul.* **2020**, *27*, 622-30. DOI
 136. Rong, Q.; Wei, H.; Huang, X.; Bao, H. Predicting the effective thermal conductivity of composites from cross sections images using deep learning methods. *Compos. Sci. Technol.* **2019**, *184*, 107861. DOI
 137. Li, S.; Xie, D.; Lei, Q. Understanding insulation failure of nanodielectrics: tailoring carrier energy. *High. Voltage.* **2020**, *5*, 643-9. DOI

138. Huang, Y.; Zhao, H.; Wang, Y.; et al. Predicting the breakdown strength and lifetime of nanocomposites using a multi-scale modeling approach. *J. Appl. Phys.* **2017**, *122*, 065101. [DOI](#)
139. Liu, D.; Li, Q.; Zhu, Y.; et al. High-throughput phase field simulation and machine learning for predicting the breakdown performance of all-organic composites. *J. Phys. D.: Appl. Phys.* **2024**, *57*, 415502. [DOI](#)
140. Liu, D.; Li, Q.; Zhu, Y.; et al. Physics-informed neural networks for phase-field simulation in designing high energy storage performance polymer nanocomposites. *Appl. Phys. Lett.* **2025**, *126*, 052901. [DOI](#)
141. Jayakrishnan, A.; Silva, J.; Kamakshi, K.; et al. Are lead-free relaxor ferroelectric materials the most promising candidates for energy storage capacitors? *Prog. Mater. Sci.* **2023**, *132*, 101046. [DOI](#)
142. Shetty, S.; Damodaran, A.; Wang, K.; et al. Relaxor behavior in ordered lead magnesium niobate ($\text{PbMg}_{1/3}\text{Nb}_{2/3}\text{O}_3$) thin films. *Adv. Funct. Materials.* **2019**, *29*, 1804258. [DOI](#)
143. Chen, J.; Qi, H.; Zuo, R. Realizing stable relaxor antiferroelectric and superior energy storage properties in $(\text{Na}_{1-x/2}\text{La}_{x/2})(\text{Nb}_{1-x}\text{Ti}_x)\text{O}_3$ lead-free ceramics through A/B-site complex substitution. *ACS. Appl. Mater. Interfaces.* **2020**, *12*, 32871-9. [DOI](#)
144. Sarkar, A.; Wang, Q.; Schiele, A.; et al. High-entropy oxides: fundamental aspects and electrochemical properties. *Adv. Mater.* **2019**, *31*, e1806236. [DOI](#)
145. Yang, B.; Zhang, Y.; Pan, H.; et al. High-entropy enhanced capacitive energy storage. *Nat. Mater.* **2022**, *21*, 1074-80. [DOI](#)
146. Chen, L.; Deng, S.; Liu, H.; Wu, J.; Qi, H.; Chen, J. Giant energy-storage density with ultrahigh efficiency in lead-free relaxors via high-entropy design. *Nat. Commun.* **2022**, *13*, 3089. [DOI](#) [PubMed](#) [PMC](#)
147. Kim, C.; Pilania, G.; Ramprasad, R. Machine learning assisted predictions of intrinsic dielectric breakdown strength of ABX_3 perovskites. *J. Phys. Chem. C.* **2016**, *120*, 14575-80. [DOI](#)
148. Mu, S.; Samolyuk, G. D.; Wimmer, S.; et al. Uncovering electron scattering mechanisms in NiFeCoCrMn derived concentrated solid solution and high entropy alloys. *npj. Comput. Mater.* **2019**, *5*, 138. [DOI](#)
149. Liu, P.; Tian, Z.; Chen, Z.; Wen, S.; Zheng, L.; Li, B. Suppressing the phase transition of ZrP_2O_7 by defect and entropy regulation for high-temperature wave-transparent material application. *J. Adv. Ceram.* **2024**, *13*, 1164-77. [DOI](#)
150. Zhu, B.; Zhang, J.; Long, F.; et al. Boosting energy-storage in high-entropy pb-free relaxors engineered by local lattice distortion. *J. Am. Chem. Soc.* **2024**, *146*, 29694-702. [DOI](#)
151. Fan, Y.; Qu, W.; Qiu, H.; et al. High entropy modulated quantum paraelectric perovskite for capacitive energy storage. *Nat. Commun.* **2025**, *16*, 3818. [DOI](#) [PubMed](#) [PMC](#)